Key Points:
- Departures from average rainfall modulated ecosystem responses in 2017 leading to intense early greening with shorter than average duration
- Access to groundwater leads to higher ET and lower water use efficiency at sites with deep-rooted riparian and mountain trees
- Low elevation sites were a seasonal carbon source, whereas a high elevation site with a lower dependance to rainfall was a carbon sink

Landscape Controls on Water-Energy-Carbon Fluxes Across Different Ecosystems During the North American Monsoon

Eli R. Pérez-Ruiz[1,2] [ID], Enrique R. Vivoni[1,3] [ID], Enrico A. Yépez[4] [ID], Julio C. Rodríguez[5] [ID], David J. Gochis[6] [ID], Agustín Robles-Morua[4] [ID], Josué Delgado-Balbuena[7] [ID], and David K. Adams[8] [ID]

[1]School of Earth and Space Exploration, Arizona State University, Tempe, AZ, USA, [2]Departamento de Ingeniería Civil y Ambiental, Universidad Autónoma de Ciudad Juárez, Ciudad Juárez, Mexico, [3]School of Sustainable Engineering and the Built Environment, Arizona State University, Tempe, AZ, USA, [4]Departamento de Ciencias del Agua y del Medio Ambiente, Instituto Tecnológico de Sonora, Ciudad Obregón, Sonora, Mexico, [5]Departamento de Agricultura y Ganadería, Universidad de Sonora, Hermosillo, Sonora, Mexico, [6]National Center for Atmospheric Research, Boulder, CO, USA, [7]Instituto Nacional de Investigaciones Forestales, Agrícolas y Pecuarias, Ojuelos de Jalisco, Jalisco, Mexico, [8]Centro de Ciencias de la Atmósfera, Universidad Nacional Autónoma de México, Ciudad de México, Mexico

Abstract The dependence of arid and semiarid ecosystems on seasonal rainfall is not well understood when sites have access to groundwater. Gradients in terrain conditions in northwest México can help explore this dependence as different ecosystems experience rainfall during the North American monsoon (NAM), but can have variations in groundwater access as well as in soil and microclimatic conditions that depend on elevation. In this study, we analyze water-energy-carbon fluxes from eddy covariance (EC) systems deployed at three sites: a subtropical scrubland, a riparian mesquite woodland, and a mountain oak savanna to identify the relative roles of soil and microclimatic conditions and groundwater access. We place datasets during the NAM season of 2017 into a wider context using previous EC measurements, nearby rainfall data, and remotely-sensed products. We then characterize differences in soil, vegetation, and meteorological variables; latent and sensible heat fluxes; and carbon budget components. We find that lower elevation ecosystems exhibited an intense and short greening period leading to a net carbon release, while the high elevation ecosystem showed an extensive water use strategy with delayed greening of longer duration leading to net carbon uptake during the NAM. Access to groundwater appears to reduce the dependence of deep-rooted riparian trees at low elevation and mountain trees on seasonal rainfall, allowing for a lower water use efficiency as compared to subtropical scrublands sustained by water in shallow soils. Thus, a transition from intensive to extensive water use strategies can be expected where there is reliable access to groundwater.

Plain Language Summary How arid and semiarid ecosystems depend on seasonal rainfall is not well understood, especially when sites have access to groundwater. We explored this topic by studying three ecosystems in northwest México which all experience summer rainfall, but have variations in groundwater access and elevation-related properties. Using the eddy covariance method, we quantified water, energy and carbon dioxide exchanges in a subtropical scrubland, a riparian mesquite woodland, and a mountain oak savanna over one summer season. We placed datasets during the summer season of 2017 into a wider context using previous measurements, nearby rainfall data, and remotely-sensed vegetation products. We found that lower elevation ecosystems had an intense and short greening period, while a high elevation ecosystem showed delayed greening of a longer duration. Those ecosystems with more abundant groundwater also had more carbon dioxide uptake during the summer. Access to groundwater appeared to reduce the dependence of ecosystems with trees on the summer season rainfall, thus allowing for longer greening periods and more carbon uptake.

1. Introduction

The North American monsoon (NAM) is characterized by increased rainfall from July to September over southwestern United States and northwestern México (e.g., Adams & Comrie, 1997; Douglas et al., 1993), leading to changes in ecosystem conditions and land-atmosphere interactions (Forzieri et al., 2011;

Méndez-Barroso & Vivoni, 2010; Pérez-Ruiz et al., 2010; Vivoni et al., 2007, 2008). Water-limited ecosystems typically respond to the onset and demise of the NAM through changes in pulses of microbial activity, leaf and canopy development, and plant photosynthesis (e.g., Biederman et al., 2018; Lizárraga-Celaya et al., 2010; Méndez-Barroso et al., 2014; Scott et al., 2010; Verduzco et al., 2018). As a result, a strong connection is presumed between the temporal distribution of rainfall during the NAM and the ecosystem processes influencing the exchange of water, energy, and carbon with the overlying atmosphere. However, it is relatively unknown, how variations in access to groundwater and microclimatic and soil conditions related to elevation might modulate these ecosystem responses.

Water-limited ecosystems have been identified as playing an important role in the carbon cycle due to their strong inter-annual variability in productivity (e.g., Ahlström et al., 2015; Poulter et al., 2014). While the NAM exhibits rainfall variability from intra-seasonal to inter-annual time scales (e.g., Cavazos et al., 2002; Higgins et al., 1999), its effect on land-atmosphere interactions, in particular carbon dioxide (CO_2) fluxes, has yet to be compared to perennial surface and subsurface water sources across different ecosystems. Widespread vegetation greening due to the synchronized availability of rainfall and solar radiation is thought to be a controlling factor on water-energy-carbon fluxes (e.g.,Forzieri et al., 2011, 2014; Méndez-Barroso et al., 2014; Vivoni et al., 2010). However, landscape controls, such as elevation effects on microclimate conditions and a consistent access to groundwater, can also play a fundamental role in differentiating the individual responses of ecosystems. Two plant greening or phenological strategies linked to intensive and extensive water use (Barron-Gafford et al., 2013; Jia et al., 2014; Lagergren et al., 2008; Rodríguez-Iturbe et al., 2001; Rodríguez-Robles et al., 2017; Scott et al., 2014; Shao et al., 2016; Wang et al., 2011, 2016) have been noted in the region through inspection of the ecosystem phenological response during the summer season. Intensive water users such as drought-deciduous species exhibit a rapid, but short period of greening after the onset of the NAM, while extensive water use strategies in primarily evergreen species favor a prolonged period of moderate greenness continuing after the NAM.

The groundwater dependence of mountain and riparian ecosystems in the NAM region is relatively unexplored, though this has been reported in other seasonally dry areas (e.g., Baldocchi et al., 2004; Paco et al., 2009). The works of Potts et al. (2008), Barron-Gafford et al. (2013), and Scott et al. (2014), for instance, identified differences between mesquite savannas growing in riparian areas versus those in upland locations and concluded that groundwater access impacted how water-energy-carbon fluxes were dependent on rainfall. Similarly, Brunel (2009) showed that riparian mesquite trees can access either soil water or groundwater depending on available rainfall and the depth to the alluvial water table. Yet, the contributions of microclimate conditions, such as air temperature, vapor pressure deficit and soil water, and the site access to groundwater, have not be elucidated. While these effects can be hard to isolate, observational studies can provide valuable insights if site differences exist across multiple landscape controls (Barron-Gafford et al., 2013; Hui et al., 2003; Rojas-Robles et al., 2020; Shao et al., 2016).

One of the challenges to assessing the dependence of water-energy-carbon fluxes to landscape controls is the difficulty of obtaining simultaneous observations in ecosystems that are generally in inaccessible areas due to rugged terrain. The eddy covariance (EC) technique (Baldocchi et al., 2001) is often used to measure fluxes at the ecosystem level, expressed in terms of the net ecosystem exchange (NEE), latent heat flux (λET), and sensible heat flux (H). A large number of independent studies have been conducted in ecosystems under the influence of the NAM, for instance in grasslands (Barron-Gafford et al., 2013; Bowling et al., 2010; Hinojo-Hinojo et al., 2016, 2019; Kurc & Small, 2007), woody savannas (Potts et al., 2010; Scott et al., 2009), riparian ecosystems (Scott et al., 2008, 2004, 2014; Williams et al., 2006; Yépez et al., 2007), shrublands (Kurc & Small, 2007; Potts et al., 2008; Vivoni et al., 2021), subtropical scrublands (Méndez-Barroso et al., 2014; Verduzco et al., 2018), semiarid woodlands (Pérez-Ruiz et al., 2010; Verduzco et al., 2015), and forests (Méndez-Barroso et al., 2014; Knowles et al., 2020). However, few studies have coordinated sampling across different ecosystems under a similar seasonal rainfall regime, but under variations in elevation and groundwater access, to identify how landscape controls might differentially impact water-energy-carbon fluxes.

Here, we conduct a field campaign in the summer of 2017 in three ecosystems in México that offered the opportunity to determine the relative roles of groundwater access and elevation-induced differences in soil and microclimate conditions. Sites were a subtropical scrubland depending on shallow soil water, a riparian

mesquite with intermediate access to groundwater, and an oak savanna with stable subsurface water in a mountain setting. Unfortunately, a high elevation site depending only on shallow soil water was not sampled. Differences in vegetation phenology (e.g., greening onset and duration, peak green-up, time-integrated green-up amount), as observed from remote sensing (Forzieri et al., 2011; Méndez-Barroso et al., 2009) for these ecosystems, suggest that a link might exist with landscape controls. While Méndez-Barroso et al. (2014) identified differences in vegetation phenology and seasonal evapotranspiration rates at two of the sites, the study was not able to distinguish sources of water nor link the plant water uptake to carbon fluxes. Thus, we deployed sensors at the subtropical scrubland and oak savanna sites that form part of the MexFlux network (Delgado-Balbuena, Arredondo, et al., 2019; Vargas et al., 2013), but which had been discontinued, and expanded observations to a third site in a riparian mesquite woodland to allow comparisons of the landscape controls described above. The new site offered the opportunity to identify how access to groundwater at a low elevation location influenced the water-energy-carbon fluxes. However, logistical restrictions of the rural sites in México constrained the field campaign to a single summer season. Nevertheless, we sampled a key period in the year which has a large contribution to annual rainfall (Douglas et al., 1993) and a preponderant role in annual carbon fluxes (Verduzco et al., 2015, 2018).

Our aim is to quantify land-atmosphere interactions during the evolution of the NAM to elucidate if (1) soil and microclimate conditions induced by variations in elevation or (2) groundwater access linked to the terrain position play a more significant role in the ecosystem response. The sampled gradient has the potential for a similar rainfall due to the close proximity of the sites (Mascaro et al., 2014). However, site variations in elevation, access to groundwater, and vegetation phenology provide a means to isolate the individual effects on the water-energy-carbon fluxes. We emphasize the CO_2 exchanges since these have not been characterized at these sites and can provide evidence on the water use strategies that have been previously inferred only from vegetation phenology and evapotranspiration (Forzieri et al., 2011; Méndez-Barroso et al., 2014). To guide our study, we posed the following questions: "What are the relative roles of soil and microclimatic conditions and access to groundwater on water-energy-carbon fluxes?" and "How are differences in these controls linked to intensive and extensive water use strategies?". In this analysis, we differentiate between near surface conditions, specifically air temperature, vapor pressure deficit and shallow soil moisture, and deeper subsurface water sources. We hypothesize that water-energy-carbon fluxes will vary significantly in the presence of stable groundwater that can provide a buffer to the high temporal variability of seasonal rainfall.

2. Methods

2.1. Study Area Description

The three EC sites were deployed in a rural, sparsely populated region in Sonora, México, arranged in a triangular pattern at ∼25-km distances (Figure 1). The sites are: (1) a subtropical scrubland (SS) located on top of an alluvial fan (29.741°N, 110.537°W) at an elevation of 622 m with thorny, deciduous trees (4 m height), shrubs, cacti, and low grass cover, with coarse, rocky soils; (2) a riparian mesquite (RM) located in a valley bottom near an ephemeral channel (29.944°N, 110.613°W) at an elevation of 681 m with tall mesquite trees (8 m height) and moderate grass cover on a coarse soil matrix; and (3) an oak savanna (OS) located in a mountain saddle (29.958°N, 110.461°W) at an elevation of 1,314 m with oak trees (5.5 m height) interspersed with grasses and succulents upon coarse, rocky soils with an abundant organic matter horizon (Ko et al., 2019; Méndez-Barroso et al., 2014). The velvet mesquite (*Prosopis velutina*) and oak (*Quercus chihuahuensis*, *Quercus oblongifolia*) trees at RM and OS, respectively, are known to have deep roots, extending beyond 2 m in depth (Baldocchi et al., 2004; Cable, 1977; Schenk & Jackson, 2002), while the understory grasses have shallow roots. At SS, grasses, shrubs, cacti, and shallow rooted trees have limited access to water below the upper soil profile (Tarín et al., 2020). Note that SS and OS are documented as part of the Mex-Flux network but had been discontinued prior to this effort (Delgado-Balbuena, Arredondo, et al., 2019; Vargas et al., 2013), while RM represents a new site with riparian characteristics not captured in MexFlux. Site conditions and their representativeness in the broader domain are shown in Figure 2. In all cases, the two-dimensional footprint for the 80% source area (Kljun et al., 2015) was within 150 m of the site in an area with homogenous vegetation for each ecosystem.
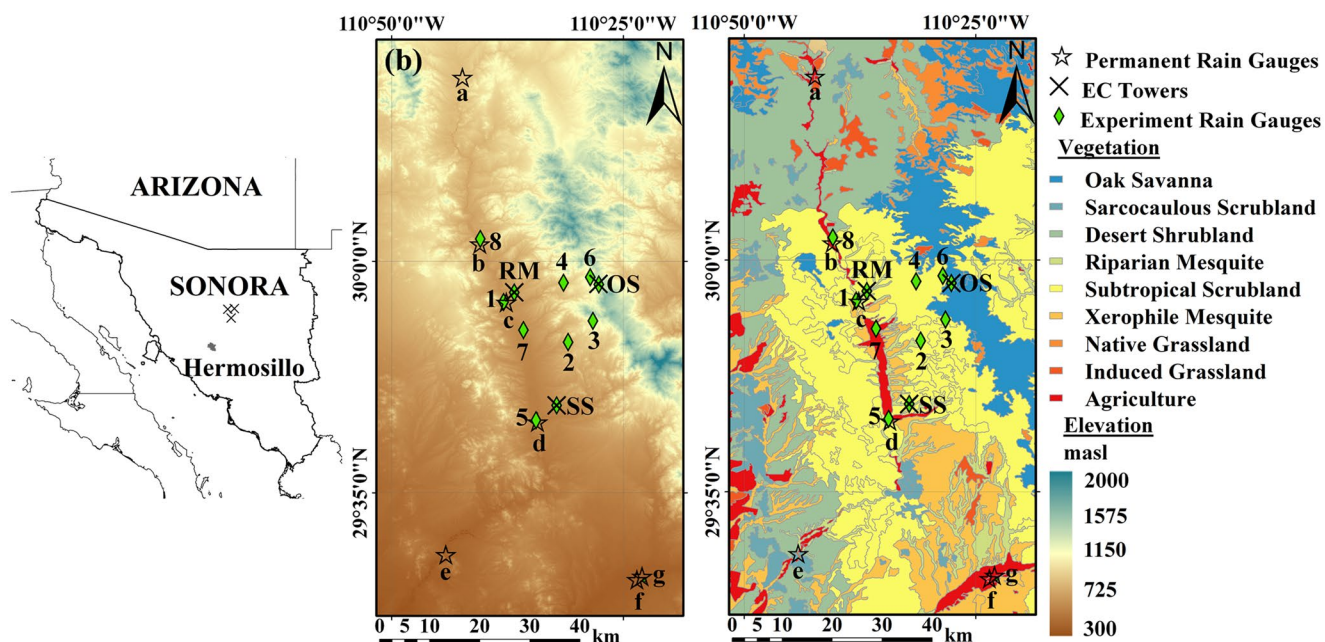
Figure 1. Location of the study sites in: (a) The state of Sonora, México and in relation to (b) Elevation, and (c) Vegetation type. Numbers and letters represent the ID of each rain gauge site. Elevation from the Continuo de Elevación Mexicano 3.0 and the vegetation type from the Conjunto de Datos Vectoriales de Uso de Suelo y Vegetación of INEGI (2016).

Climate in the area is classified as steppe or semiarid (BhS) according to Köppen-Geiger (Peel et al., 2007), characterized by hot, arid conditions; winter temperatures above 0°C; and warm season rainfall (*R*). According to seven permanent rain gauges in the region (Table 1), the mean annual rainfall is 469 mm per year, with more than 65% occurring during the NAM (July, August, and September). Daily visual measurements of rainfall are made at permanent rain gauges by the Comisión Nacional de Agua (CONAGUA) in small towns at low elevations. To complement these observations, a network of 11 continuous, tipping-bucket rain gauges (TE525, Texas Electronic, Dallas, TX) were deployed during the field campaign at elevations ranging from 558 to 1,462 m (Table 1). Three of these rain gauges are co-located with the EC sites, while the remainder allow for characterizing the spatial variability of rainfall in the region.

2.2. Eddy Covariance Measurements and Data Processing

High frequency measurements of water, energy, and carbon fluxes were obtained with the EC method (Baldocchi, 2003). EC systems consisted of an infrared gas analyzer (IRGA) to measure H_2O and CO_2 concentrations and a sonic anemometer to measure wind components. The IRGA consisted of a LI-7500 for SS and RM, and a LI-7500RS (both from Li-COR Biosciences, Lincoln, Nebraska) for OS. The sonic anemometers were a CSAT-3 (Campbell Scientific, Logan, Utah) for SS and RM, and a Windmaster Pro (Gill Instruments, Hampshire, UK) at OS. EC systems were installed at 9, 12, and 9 m above the ground surface at the SS, RM, and OS sites, respectively. Fluxes were calculated at 30-min intervals with the software EddyPro® 6.2.0. An initial quality check was performed consisting of a spike detection and a removal procedure using a maximum of three consecutive outliers (Vickers & Mahrt, 1997) and outliers greater than 3 standard deviations (std) for gas concentrations and 5 std for wind components (Schmid et al., 2000), and an amplitude resolution with a range of variation above 7 std (Vickers & Mahrt, 1997). We set initial absolute limits for zonal velocity (-30–30 m s^{-1}), meridional velocity (-5–5 m s^{-1}), sonic temperature (-20°C–50°C), CO_2 concentration (200–600 μmol mol^{-1}), and H_2O concentration (0–40 mmol mol^{-1}).

Flux processing included detrending by block averaging and time lag compensation by covariance maximization (Massman, 2001; Moncrieff et al., 1997), axis rotation by double rotation (Wilczak et al., 2001), low-frequency correction using the analytical correction of high-pass filtering effects (Moncrieff et al., 2004), corrections for stability and density fluctuations (Foken et al., 2006; Webb et al., 1980), and estimates of
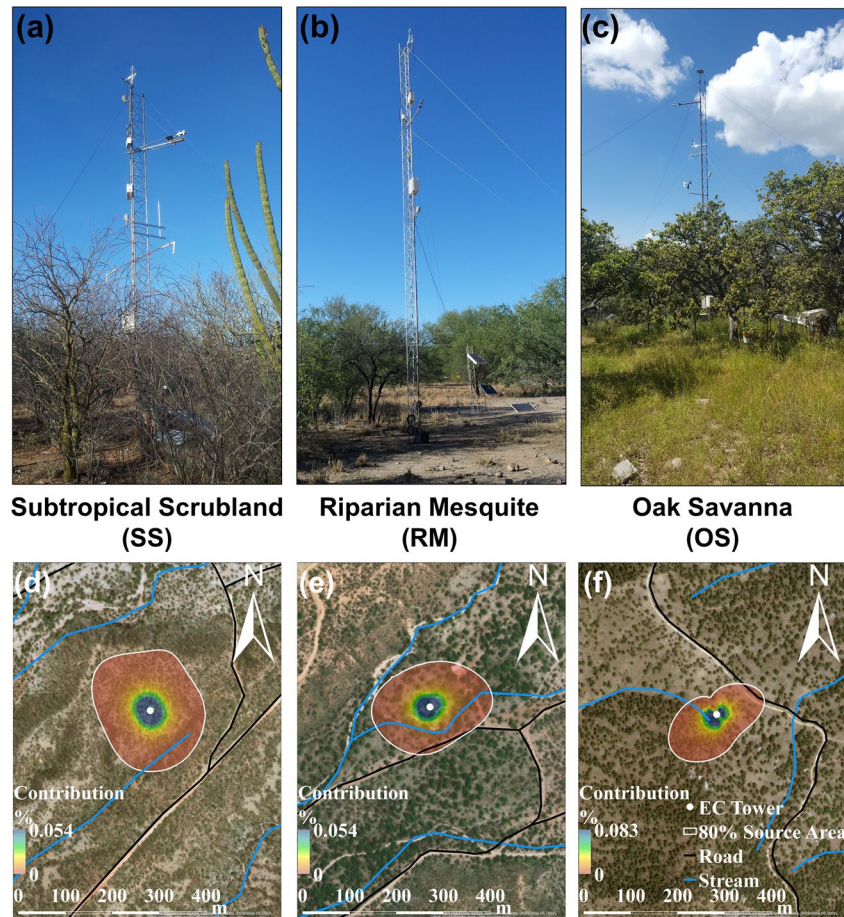
Figure 2. Photographs showing the EC sites and the ecosystems at the three sites: (a) Subtropical Scrubland, (b) Riparian Mesquite, and (c) Oak Savanna. (d), (e), and (f) show the 80% footprint source area (colors are percent contribution of each 1-m pixel) of the area around each EC site. EC, eddy covariance.

sensible heat were obtained from the sonic temperature (Paw U et al., 2000). An angle of attack correction (Nakai & Shimoyama, 2012) was applied at the OS site. Average half-hour corrected fluxes were also filtered to exclude periods with rainfall ($R > 0.2$ mm per 30-min) and when winds were ±10° from the opposite direction of the mounted instruments. Range limits were set for net ecosystem exchange (NEE ± 1.3 mg CO_2 m^{-2} s^1), latent heat flux (λET from −50–450 W m^{-2}), and sensible heat flux (H from 200–800 W m^{-2}), following the procedures of Schmid et al. (2000). Finally, fluxes were filtered using a friction velocity criterion of $u^* < 0.10$, 0.14, and 0.24 m s^{-1} for SS, RM, and OS, to exclude spurious data under stable atmospheric conditions. The u^* thresholds were estimated using the Moving Point Test (Papale et al., 2006). Gap filling of the flux data was applied using the methods of Reichstein et al. (2005) through the tool REddyProc (Wutzler et al., 2018). During the sampling period, there were about 29% (SS), 49% (RM), and 45% (OS) of missing data due to sensor failures, quality control, and other maintenance issues. Generally, gaps were evenly distributed throughout the study period, except at RM where a 23-days gap was present from mid-July to mid-August due to major physical damage at the site.

To complement the NEE measurements, we estimated ecosystem respiration (R_{eco}) and gross primary productivity (GPP) using a flux partitioning tool in REddyProc. GPP and R_{eco} allow distinguishing the temporal behavior on ecosystem carbon uptake and release, respectively. This procedure was based on the nighttime sensitivity of NEE to air temperature (T_{air}) using the exponential regression model of Lloyd and Taylor (1994) as:

Table 1
Characteristics of the Campaign and Permanent Rain Gauge Sites

	Campaign rain gauges						
ID	Rain gauge site	Longitude (dd)	Latitude (dd)	Elevation (m)	Start period	End period	Summer R (mm)
1	Opodepe	−110.631	29.927	639	5/15/17	11/17/17	294.9
2	El Saucito	−110.516	29.855	812	5/15/17	11/18/17	334.5
3	El Tule	−110.471	29.893	1,118	5/15/17	11/18/17	542.0
4	La Ramada	−110.524	29.962	852	5/15/17	11/17/17	322.8
5	Rayon	−110.573	29.714	558	5/15/17	11/17/17	244.6
6	Sierra Los Locos	−110.476	29.972	1,268	5/15/17	11/8/17	277.4
7	Santa Margarita	−110.596	29.876	622	6/15/17	9/28/17	560.6
8	Meresichic	−110.673	30.040	721	6/15/17	9/28/17	250.4
SS	*Subtropical Scrubland*	−110.537	29.741	622	6/11/17	10/7/17	275.4
RM	*Riparian Mesquite*	−110.613	29.944	681	5/29/17	10/9/17	260.1
OS	*Oak Savanna*	−110.461	29.958	1,462	5/24/17	10/8/17	254.2

	Permanent rain gauges					
ID	Rain gauge site	Longitude (dd)	Latitude (dd)	Elevation (m)	Period	Summer R (mm)
a	Cucurpe	−110.706	30.331	853	1967–2011	315.4
b	El Cajon	−110.736	29.472	390	1974–2011	290.5
c	Meresichic	−110.675	30.031	712	1980–2011	345.4
d	Opodepe	−110.627	29.926	663	1944–1983	314.8
e	Rayon	−110.571	29.711	560	1974–2011	334.9
f	Ures SMN	−110.383	29.433	397	1921–1977	323.8
g	Ures	−110.392	29.427	385	1978–2011	276.1

Note. Summer R determined from 06/15/2017 to 09/28/2017 at all sites. Italics represent the three EC sites.

$$R_{eco}\left(T_{air}\right) = R_{ref}\,e^{E_0\left(\frac{1}{T_{ref}-T_0} - \frac{1}{T_{air}-T_0}\right)}, \tag{1}$$

where R_{ref} is the reference respiration at T_{ref} (10°C), T_o equals −46.02°C, and E_o is an activation energy parameter (207.30, 250.53, and 165.81 K for SS, RM, and OS, respectively). In addition, we compared estimates of λET, H, and NEE at SS and OS to other available summer periods to quantify the representativeness of the conditions during the 2017 NAM season. At SS, summer datasets were averaged from 2008 to 2012, while OS was captured by averaged summer data from 2008 to 2014. As part of the quality control, we inspected the energy balance closure ($\varepsilon = \sum(H + \lambda$ET$) / \sum(R_n - G)$) for periods of simultaneously available fluxes (Table 2), finding that 65%–90% of the available energy ($R_n - G$) was measured as turbulent fluxes ($H + \lambda$ET). A lack of G measurements at OS throughout the study period (assumed $G = 0$) impacted the energy balance closure at this site. Overall, these results are within the range of other EC studies (34%–169%) across different ecosystems (Wilson et al., 2002). Similarly, a regression of the form $H + \lambda$ET $= m(R_n - G) + b$ was performed, finding values of m and b that were generally within those reported (m from 0.55 to 0.99, b from −32.9 to 36.9) by Wilson et al. (2002).

Table 2
Energy Balance Closure Using Two Techniques

Site	ε	Slope (m)	Intercept (b)	R^2
Subtropical Scrubland	0.92	0.64	53.97	0.84
Riparian Mesquite	0.87	0.72	27.60	0.86
Oak Savanna	0.65	0.52	25.43	0.83

Note. (1) ε or the Ratio of the Sum of ($H + \lambda ET$) to the Sum of ($R_n - G$), and (2) Linear Fit ($H + \lambda ET = m(R_n - G) + b$) With Slope ($m$), Intercept ($b$), and Coefficient of Determination (R^2). Note that OS had no G measurements (assumed zero).

2.3. Ancillary and Remotely-Sensed Datasets

Additional ancillary meteorological and soil measurements were obtained for each site, including: (1) air temperature (T_{air}) and relative humidity (RH) using a HMP45C sensor at SS, and a HMP155A sensor (both from Vaisala, Helsinki, Finland) at RM and OS; (2) net radiation (R_n) with a CNR2 sensor at SS and RM, and a CNR4 sensor (both from Kipp & Zonen, Delft, The Netherlands) at OS; and (3) soil water content using CS616 sensors (Campbell Scientific, Logan, Utah) at 5, 15, and 30 cm depths at RM and a set of HydraProbes (Stevens, Portland, Oregon) at 5 and 15 cm depths at SS and at 15 cm depth at OS, respectively. Due to the use of the CNR2 sensor, incoming solar radiation (R_s) was not measured at SS and RM. Nevertheless, a comparison of R_s from previous observations at SS and OS showed no statistically significant difference in energy input across the elevation gradient. Ground heat flux (G) was only available at SS and RM using a HFP01-L sensor with corrections made with soil thermometers (both from Campbell Scientific, Logan, Utah) at 2 and 4 cm. No measurements of G were obtained at OS. Volumetric soil water content values were converted to a relative water content (s) dividing by the maximum value at each site. Vapor pressure deficit (VPD) was calculated using T_{air} and RH.

In addition, we used remotely-sensed data on the Normalized Difference Vegetation Index (NDVI) derived from the Moderate Resolution Imaging Spectroradiometer (MODIS) surface reflectance composites (MOD09A1; ORNL DAAC, 2018) at 500-m pixel and 8-days resolution. NDVI observations, over the period of January of 2001 to December of 2018 were used for three purposes: (1) to estimate the temporal variation of vegetation greenness for the 500-m pixel containing each EC site during the field campaign, (2) to obtain the ecosystem-average conditions during the summer of 2017 for pixels corresponding to the same vegetation type as in the EC sites (INEGI, 2016), and (3) to estimate the long-term (2001–2018) conditions of vegetation greenness at the EC sites. For these purposes, NDVI was found to be suitable and we found no significant differences when inspecting the Enhanced Vegetation Index (EVI) in the region (Méndez-Barroso et al., 2009). In a similar fashion, we used rain gauges for two purposes: (1) to obtain the long-term monthly R at seven permanent locations, and (2) to calculate daily and monthly R for the summer of 2017 at 11 locations, including the EC sites.

2.4. Data Analysis

The study period was divided into four NAM stages for summer 2017: (I) pre-monsoon corresponding to the dry season when the vegetation was dormant, (II) early monsoon when the onset of rainfall promoted soil biological activity and canopy development, (III) late monsoon considered to be the maximum plant activity, and (IV) post-monsoon when leaf senescence began and ecosystems returned to dormancy. Note that labels I through IV are used to refer to these stages. Dates of the NAM stages began from Day of Year (DOY) 162, 149, and 144 for SS, RM, and OS, and extend as: (I) up to July 1 (DOY 182), (II) from July 2 to 19 (DOY 183–200), (III) from July 20 to August 28 (DOY 201 to 240), and (IV) after August 29 (DOY 241). The stages were selected to capture rainfall onset and the different responses of ecosystems during the NAM. The large gap at RM corresponded to stage III. For each stage, we conducted analyses of the daily variations of water-energy-carbon fluxes. Seasonal averages of daily meteorological variables (T_{air}, VPD, and RH), energy fluxes (H and λET), and carbon fluxes (NEE, R_{eco}, and GPP) were compared using the Kruskal-Wallis One Way Analysis of Variance on Ranks (ANOVA). Statistical analyses of the fluxes included daily values obtained from gap-filled data, whereas we excluded days with missing data from analyses of meteorological variables. If statistical significance was found ($p < 0.001$), the All Pairwise Multiple Comparison Procedures (Dunn's Method) was applied to find differences between the sites.

To evaluate the effects of landscape controls, we calculated the Inherent Water Use Efficiency (IWUE), the evaporative index (EI), and the evapotranspiration from groundwater (ET_{gw}) index at each site. IWUE is obtained at the ecosystem level as IWUE = (GPP*VPD)/ET, and considers carbon assimilation per unit of ecosystem water use, while accounting for the atmospheric water demand (Beer et al., 2009). EI or ET/R is the fraction of rainfall consumed by ET (Budyko, 1974). Water-limited ecosystems often exhibit a high EI, which can exceed unity if other water sources such as groundwater are used (Williams et al., 2012). ET_{gw} is the component of ET from groundwater obtained from a water budget approach that assumes an effective soil depth. Westenburg et al. (2006) showed that $ET_{gw} = ET - R + Z_r\Delta S$, where $Z_r\Delta S$ is the change in soil water storage (ΔS) over the soil depth (Z_r), assumed here as 40 cm at all sites due to the soil water measurement depths (Schreiner-McGraw & Vivoni, 2018), when there is negligible runoff (Q) and deep percolation (P). While runoff measurements are not available at the sites, arid and semiarid ecosystems in
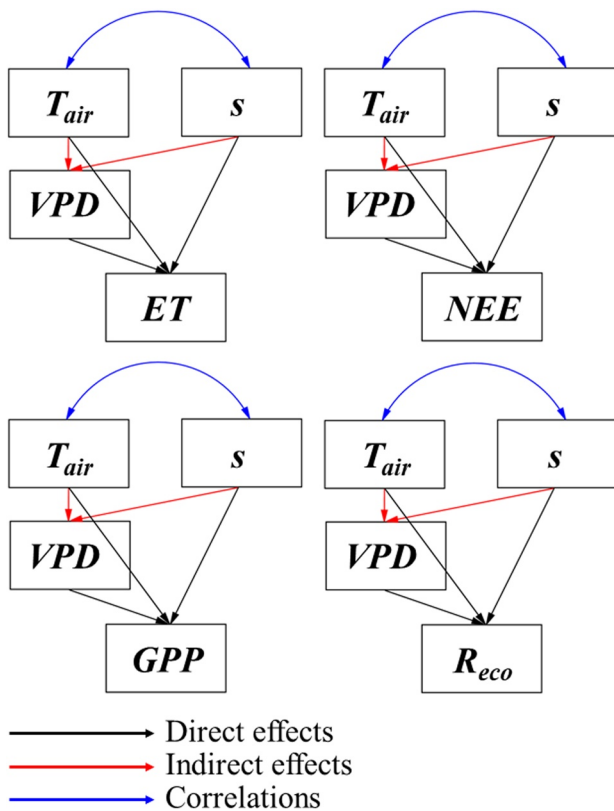
Figure 3. Path analysis scheme used to explore relations between environmental conditions (T_{air}, VPD, and s) and ET and carbon fluxes (NEE, GPP, and R_{eco}). GPP, gross primary productivity; R_{eco}, ecosystem respiration; NEE, net ecosystem exchange; VPD, Vapor pressure deficit.

the region generally have low Q relative to R and ET due to coarse and rocky soils as classified by INEGI (2016) (e.g., Yermosol at SS, Fluvisol at RM, and Lithosol at OS; all of coarse nature with sandy loam textures, Méndez-Barroso et al., 2014). For instance, Vivoni et al. (2021) document long-term average Q/R values ranging from 3% to 7% in a mixed shrubland and a mesquite savanna. Thus, total evapotranspiration can be decomposed into contributions from groundwater (ET_{gw}) and soil water ($ET_s = R - Z_r \Delta S$), or simply $ET = ET_{gw} + ET_s$. We derived uncertainty estimates following the approach of Scott (2010) for rain gauge underestimation ($R_c = 1.05\,R$), the approach of Twine et al. (2000) for deriving an energy closure-forced evapotranspiration term ($ET_f = ET/\varepsilon$), and the effect of a larger soil depth ($2Z_r$ or 80 cm) on ET_{gw}. It is recognized that the use of ET_f is conditioned on energy balance closure errors (Table 2), but is considered appropriate here for bounding the range of values of ET_{gw}.

We performed a path analysis (PA) to explore the direct and indirect relations between environmental conditions and fluxes. PA is useful when previous correlative information is known between multiple variables (e.g., Huxman et al., 2003; Li et al., 2017; Monson et al., 2005). The standardized path coefficient (β) was used to quantify the effect size of one variable on another (Shao et al., 2016). Our tests were developed to explore the effect of soil and meteorological variables on the daily values of ET, NEE, R_{eco}, and GPP based on prior studies using this methodology (Hui et al., 2003; Huxman et al., 2003; Saito et al., 2009; Wang et al., 2016). The approach included the direct effects of T_{air}, VPD, and s on the fluxes, the indirect effects of T_{air} and s on VPD, and the correlations between T_{air} and s, as shown in Figure 3. Despite significant correlations, we excluded testing the direct effects of a soil or meteorological variable on another (e.g., s direct effect on T_{air}) to focus on how the soil and microclimatic conditions at each site influenced the fluxes. An ANOVA was performed to test the statistical significance of the regressions in the PA. All statistical analyses were performed using SPSS Statistics 26.

3. Results

3.1. Rainfall and Vegetation Seasonality

As a first step, we analyzed the seasonal variation of rainfall and vegetation greenness during 2017 in relation to the long-term behavior from CONAGUA and MODIS data. Notably, the total summer R were similar at all EC sites (276, 261, and 258 mm for SS, RM, and OS, respectively), while greater variability (329 ± 114 mm)

Table 3
Comparison of Daily Rainfall Event Sizes During Sampling Period at Each Site

Rainfall event size	SS		RM		OS	
	Days	% R	Days	% R	Days	% R
$R = 0$ mm d^{-1}	82	0	90	0	95	0
0 mm d$^{-1} < R \le 5$ mm d^{-1}	23	12.20	33	18.24	35	15.75
5 mm d$^{-1} < R \le 15$ mm d^{-1}	10	32.17	3	8.93	5	18.15
15 mm d$^{-1} < R \le 25$ mm d^{-1}	3	19.83	5	37.90	0	0.00
$R > 25$ mm d^{-1}	3	35.80	3	34.92	3	66.10
All Events	121	100	134	100	138	100

OS, oak savanna; RM, riparian mesquite; SS, subtropical scrubland.
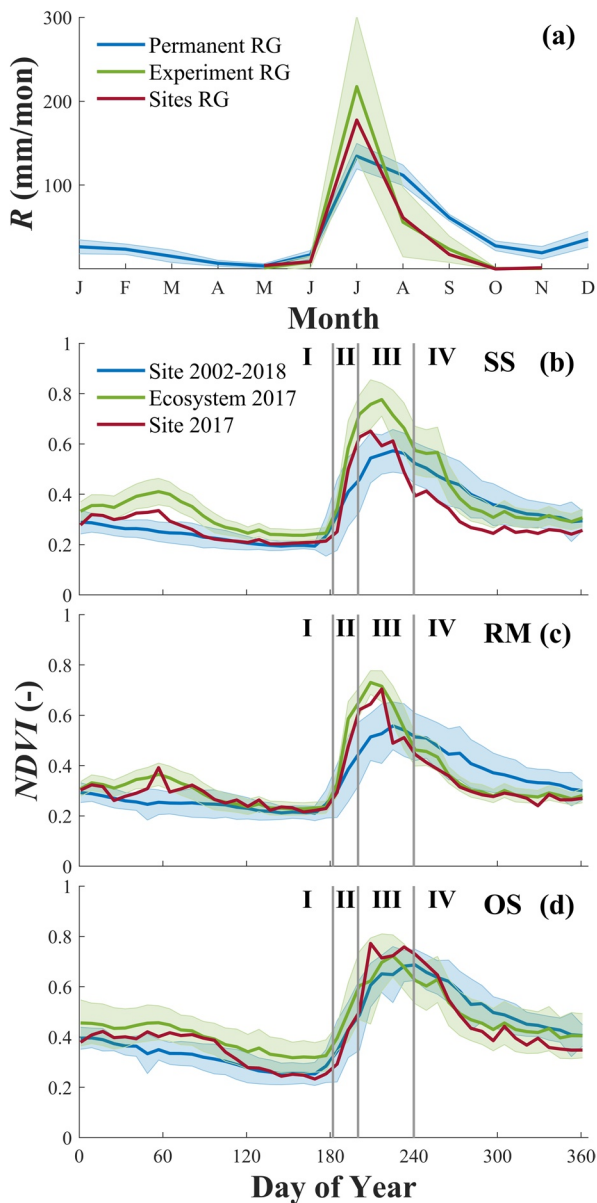
Figure 4. (a) Monthly R at EC sites ("Sites RG") and campaign rain gauge network ("Experiment RG", with average and ±1 temporal standard deviation) in comparison to long-term monthly R at permanent rain gauges ("Permanent RG", with average and ±1 standard deviation). (b-d) Monthly NDVI from 2017 at the three sites ("Site 2017"), the long-term NDVI at sites ("Site 2002–2018", with average and ±1 standard deviation), and the ecosystem average NDVI for 2017 ("Ecosystem 2017", with average and ±1 spatial standard deviation). EC, eddy covariance; NDVI, normalized difference vegetation index.

was found across the rain gauge network (Table 1). The EC sites had a similar number of rainfall events of a particular size, as shown in Table 3. At OS, however, more precipitation occurred during large events ($R > 25$ mm d^{-1}). Overall, these differences can be considered small given the large spatial variations in rainfall in the network. To illustrate this, Figure 4 presents the monthly rainfall (R) during the summer of 2017 in comparison to the long-term data. At the campaign rain gauges, the month of July in 2017 had considerably more rainfall than the long-term average (132% and 162%), while rainfall in August and September of 2017 were below average (both 45%). As a result, vegetation greening in 2017 exhibited anomalous behavior with respect to the long-term average, as shown using NDVI for the EC sites and for the areas occupied by their respective ecosystems in Figure 4. We note that greening in 2017 occurred earlier than average (in July) at all EC sites, with a more pronounced effect at SS and RM. Similarly, the early demise of the NAM (i.e., below average rainfall in August and September) led to an earlier onset of dormancy relative to the long-term trend. In the case of OS, the ecosystem showed a slightly above average greening during most of the NAM season, despite the lower monthly R during August and September.

The vegetation response at the EC sites was consistent with the variability across similar vegetation types in the region during 2017, as shown in Figures 4b–4d. At SS, the ecosystem average was higher than the EC site, likely due to the spatial variation of rainfall in the large extent of subtropical scrublands. To explore this further, we created NDVI maps for 2017 and compared these to long-term averaged conditions based on NDVI difference maps (2017 minus 2002–2018) as shown in Figure 5. During May and June, NDVI values were low, except in high elevation sites, while differences with the long-term average conditions were small. In July, a large increase in NDVI occurs in response to the NAM onset (note the 8-days rainfall totals from 12 to 166 mm). Given the above average rainfall, vegetation greening in July 2017 for RM and SS was greater than the long-term average (123% and 117%), while OS was similar to the long-term average. In August, an initial decrease of NDVI occurs in subtropical scrublands in southern areas and then spreads during September to all low elevations. As compared to the long-term average, these two months have lower NDVI for RM and SS (90% and 86%), indicating a more rapid senescence during 2017, except at higher elevations (OS) where there is more persistent greenness.

3.2. Daily Variations in Meteorological Conditions

Figure 6 presents daily meteorological and soil variables at the three EC sites, while Table 4 presents averages over stages II, III, and IV, selected to focus on monsoon conditions. Storm events generally led to a decrease in T_{air} and an increase in RH at the three sites, in particular during stage II (early monsoon). As expected, the higher elevation OS site (average T_{air} of 23.85°C) was cooler than the lower elevation SS and RM sites (average T_{air} of 28.4 and 27.32°C, $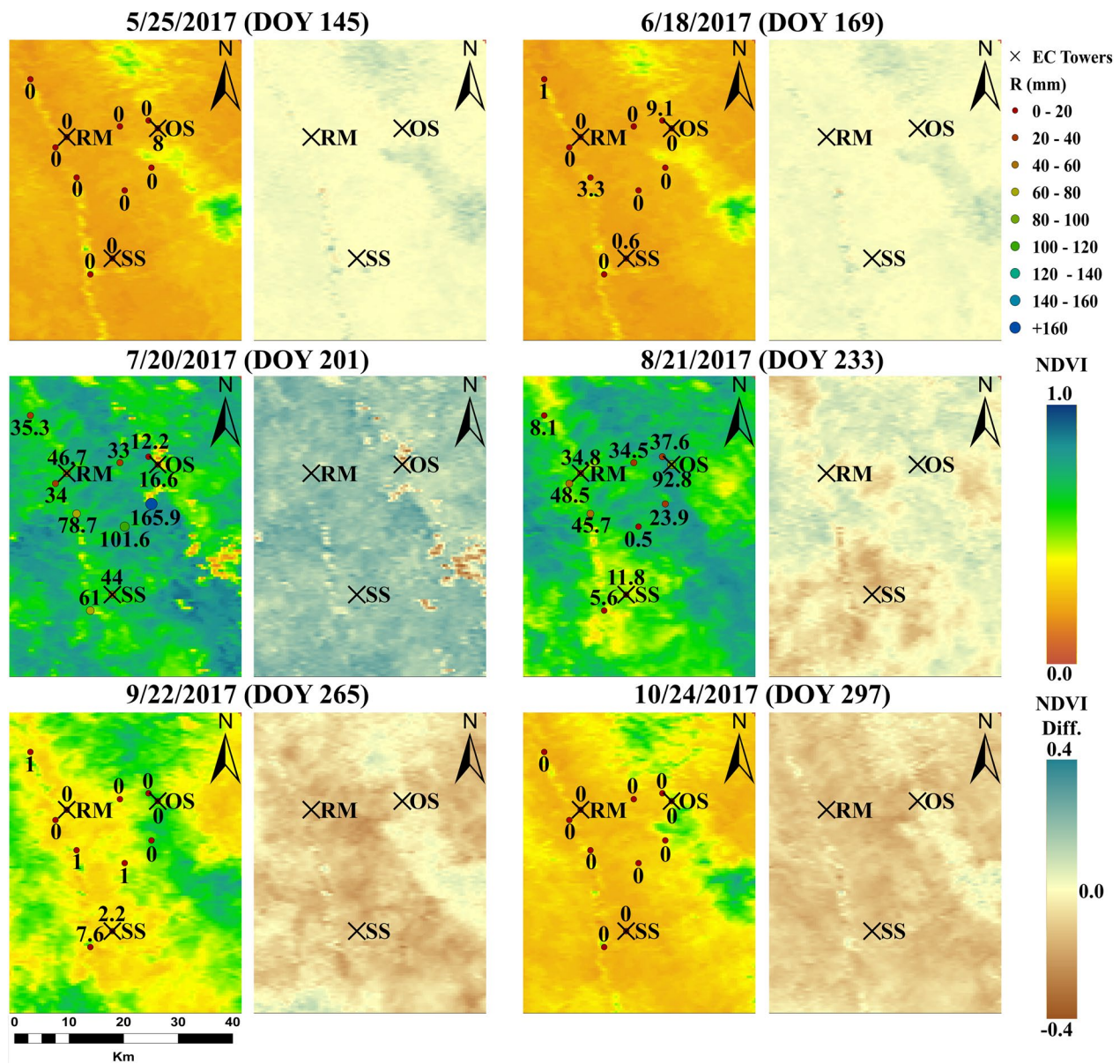p < 0.01$). Daily-average values of RH and VPD showed differences that are statistically significant between SS and the other sites (Table 4). Even though gaps were present in R_n values at SS and RM, a similar daily variability of R_n was noted ate the three sites. Daily R_n were somewhat lower at SS and RM (average of 138 and 143 W m^{-2}) than at OS (average of 167.5 W m^{-2}). s exhibited a strong seasonality reflecting the overall wetting and drying during the NAM. Note that SS exhibited more rapidly depleted soil water as compared to RM and OS, an indication of differences in soil water losses by the ecosystems, including evapotranspiration.

Figure 5. Variation of NDVI from May 25, 2017 to October 24, 2017. For each date, the image pair shows MODIS NDVI 8-days composite values (left) and the difference between each image and the MODIS long-term NDVI average during 2002–2018 (right). Circles represent the sum of R during the 8-day period with values labeled using numbers. MODIS, Moderate Resolution Imaging Spectroradiometer; NDVI, normalized difference vegetation index.

3.3. Response of Water-Energy-Carbon Fluxes

We present the total seasonal values of R, ET, and NEE in Table 4. While R was similar at the sites, ET varied considerably, suggesting that different water use strategies existed across the sites. Total NEE during the season also varied substantially. SS and RM behaved as net carbon sources, while the OS site was a net carbon sink. A gradient was noted across the sites, with GPP increasing in the order of SS, RM, and OS and exhibiting statistical differences, while R_{eco} was statistically similar at RM and OS, but lower and statistically different at SS.

Figure 7 presents daily totals of R and NEE, daily averages of λET and H, and 8-days composite values of NDVI. During the pre-monsoon (I), values of λET, NEE, R_{eco}, GPP, and NDVI were close to zero due to vegetation dormancy, while maximum values of H occurred. In the early monsoon (II), rainfall and increased
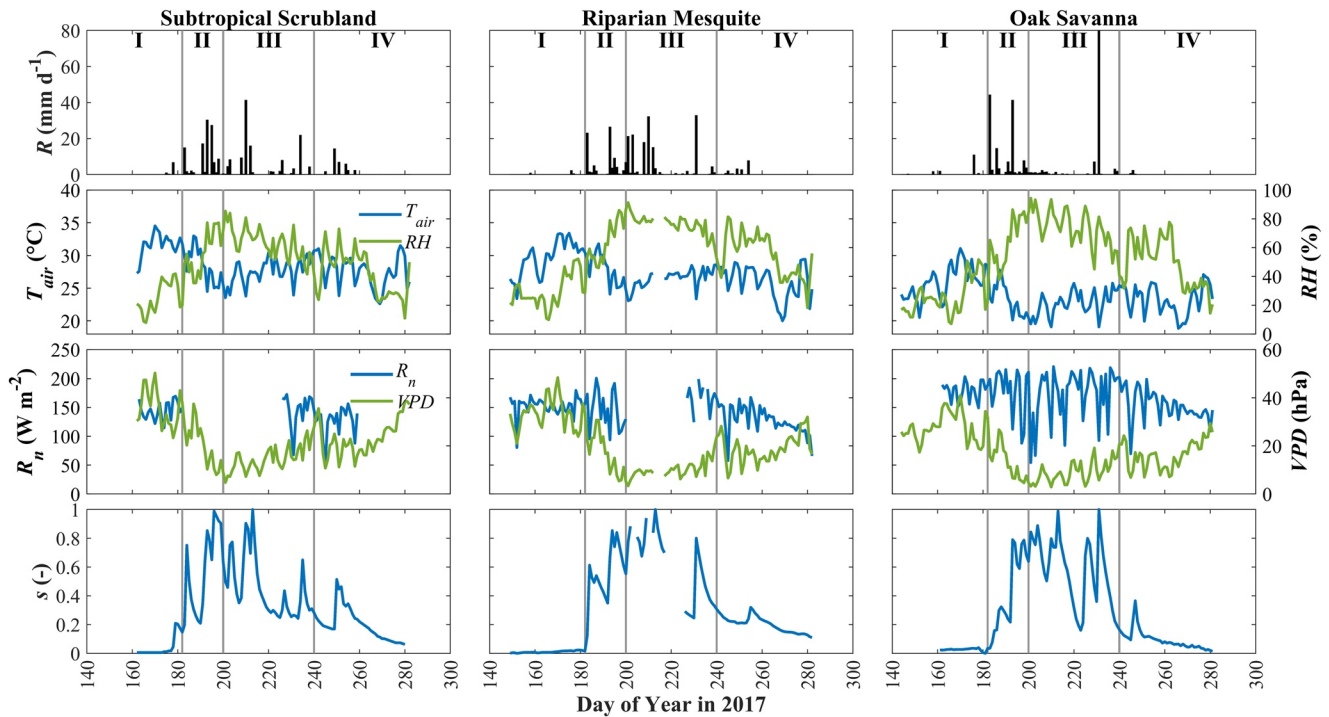
Figure 6. Daily variations in rainfall (R), air temperature (T_{air}), relative humidity (RH), net radiation (R_n), vapor pressure deficit (VPD), and relative water content (s) at the three study sites in the NAM stages of: (I) pre-monsoon, (II) early monsoon, (III) late monsoon, and (IV) post-monsoon. NAM, North American monsoon; VPD, Vapor pressure deficit.

soil water content led to an increase in λET followed by a decrease in H, and a positive NEE resulting from an increase of R_{eco} with the first storms. Fluxes in stage II were similar to previous years at SS and OS, such that initially 2017 had a behavior similar to average conditions. In the late monsoon (III), maximum NDVI at each EC site resulted in persistently high λET and low H, while GPP was higher than R_{eco}, leading to CO_2 uptake, with values of NEE of about -20 and -14 g CO_2 m^{-2} d^{-1} for SS and OS. At RM, periods of CO_2 uptake and release occurred with a similar frequency, leading to NEE near zero.

As NDVI decreased in the post-monsoon (IV), changes were noted in λET, H, and NEE, with larger variations between the ecosystems. Recall that below average rainfall and NDVI were noted for August and September. As a result, NEE values close to zero were measured at SS, which was more carbon neutral than the long-term average conditions (2008–2012), due to the sudden increase of R_{eco} from a weak reactivation from storm events in the late monsoon (III). In contrast, the OS site remained active throughout stage IV, with above average NDVI and higher NEE values as compared to previous years (2008–2014). GPP and R_{eco} showed a clear distinction among the sites in the post-monsoon that provide insight into the plant water use strategies and the phenological differences between the sites. At SS, there was a marked decrease of GPP and R_{eco} in September, in response to the end of rainfall. In contrast, RM and OS were able to sustain levels of GPP and R_{eco} for longer periods, possibly due to additional water sources, with a more notable extension at OS, where GPP was maintained for a longer period and had higher values than R_{eco}, leading to positive NEE. The variations of the carbon flux components highlighted clearly the ecosystem differences as compared to prior work that relied solely on ET and NDVI.

3.4. Landscape Controls Along Ecosystem Gradient

Next, we quantified the landscape controls related to elevation-induced soil and microclimate conditions for stages II, III, and IV using the path analysis (Table 5). Since T_{air} varied significantly across the sites, it has a significant direct contribution to ET, R_{eco}, and GPP, with increases in these fluxes at higher air temperatures. NEE did not exhibit a significant dependence on T_{air} but showed a positive relation at all sites. While VPD

Table 4

Comparison of Seasonal Values of Meteorological Variables, Turbulent Fluxes, Water Budget, and Carbon Budget Across the Three Sites for Stages II, III, and IV

	SS[a]	RM[b]	OS[c]
Meteorological Variables			
T_{air} (°C)	28.40[a]	27.32[b]	23.85[c]
RH (%)	48.27[a]	55.24[bc]	51.65[bc]
VPD (hPa)	22.15[a]	19.95[bc]	17.00[bc]
Turbulent Fluxes (W m^{-2})			
λET	54.65[a]	60.85[bc]	62.91[bc]
H	83.80[a]	66.68[b]	50.53[c]
Water Budget (mm)			
ET	228.54[a]	273.40[bc]	300.05[bc]
ET$_f$	244.48[ab]	319.96[abc]	406.73[bc]
R	276.00[abc]	260.87[abc]	257.80[abc]
$Z_r\Delta S$	0.21[ac]	5.28[ab]	−0.50[ac]
Carbon Budget (g CO$_2$ m^{-2})			
NEE	9.56[ab]	151.66[ab]	−299.25[c]
R_{eco}	1601.00[a]	2712.31[bc]	2753.21[bc]
GPP	1591.46[a]	2560.57[b]	3052.42[c]

Note. The use of superscript a, b and c for SS, RM, and OS, respectively, indicate groupings with no statistically significant differences, if used together.

GPP, gross primary productivity; NEE, net ecosystem exchange; OS, oak savanna; RM, riparian mesquite; SS, subtropical scrubland; VPD, Vapor pressure deficit.

could be considered a critical factor, significant differentiation was only noted between SS and the other sites (Table 4). Higher VPD was negatively correlated with ET, R_{eco}, and GPP in the three ecosystems, generally at significant levels. However, NEE had a limited dependence on VPD. The RM sites showed a positive and significant effect, but the SS and OS sites exhibited no significant effect of VPD on NEE. This implies that the seasonality noted in VPD only impacts NEE at RM, whereas the other sites have temporal variations that did not resemble VPD. Finally, soil water content had a significant direct and positive effect on ET. However, the strength and significance of this effect decreased from SS, to RM, and to OS, indicating less dependence on shallow soil water for evapotranspiration. Furthermore, NEE dependence on s varied among the sites. For SS, there was no significant direct effect of s on NEE, while the RM and OS sites showed similar positive effects such that higher s led to a higher NEE. Underlying these variations in NEE are differences in the direct effect of s on R_{eco} and GPP across the ecosystem gradient.

To assess the effect of groundwater access, we present values of EI and ET$_{gw}$, as well as their uncertainty estimates, and IWUE for stages II, III, and IV in Table 6. EI showed a clear difference along the gradient. SS had values of EI less than unity, such that the ecosystem had lower ET than R, even when accounting for measurement uncertainty. At both RM and OS, EI was equal to or greater than 1, indicating that a water source in addition to R was used. This is consistent with positive ET$_{gw}$ estimates for all cases at RM and OS, including those with $2Z_r$. The robustness of positive ET$_{gw}$ to the various sources of uncertainty suggest that RM and OS could have consumed water from deeper soil layers. Potential differences in water sources also impacted water use efficiency as measured by IWUE. During the early monsoon (II), similar IWUE values were noted along the ecosystem gradient due to rainfall availability and low atmospheric water demand. By stage IV, IWUE displays clear differences that could be related to access to groundwater since SS showed the highest IWUE and had low soil water during the post-monsoon. Since the elevation at SS and RM was similar, but IWUE in stage IV exhibit large differences with less efficiency at RM, soil and microclimate conditions have a smaller effect on water use efficiency as compared to groundwater access.

4. Discussion

4.1. Water-Energy-Carbon Fluxes Along Ecosystem Gradient

Prior efforts have characterized ecosystem responses to seasonal NAM rainfall using remotely-sensed vegetation indices and evapotranspiration measurements (e.g., Forzieri et al., 2011; Méndez-Barroso et al., 2014). While useful, these evaluations have limitations in their ability to distinguish the relationship between water and carbon fluxes which are essential to identifying water use patterns in arid and semiarid regions (e.g., Barron-Gafford et al., 2013; Scott et al., 2014). By inspecting conditions along an ecosystem gradient, we identified the variations of microclimatic conditions, access to groundwater, intensive or extensive phenology, and seasonal carbon fluxes under similar rainfall conditions. Figure 8 presents a summary for the sampled gradient along which both T_{air} and VPD decrease (from left to right), though access to groundwater varies with landscape position. Net seasonal carbon budgets along the gradient also depend on the relative growth rates of GPP and R_{eco}. Subtropical scrublands appear dependent on shallow soil water from rainfall events due to their placement in alluvial fans that have deep groundwater. Riparian mesquite and oak savanna sites seem to have access to subsurface water stored in an alluvial aquifer and within a fractured rock aquifer, respectively. The lack of groundwater in subtropical scrublands leads to a high dependence on seasonal rainfall variability, leading to an intensive phenological pattern, as well as a dependence on
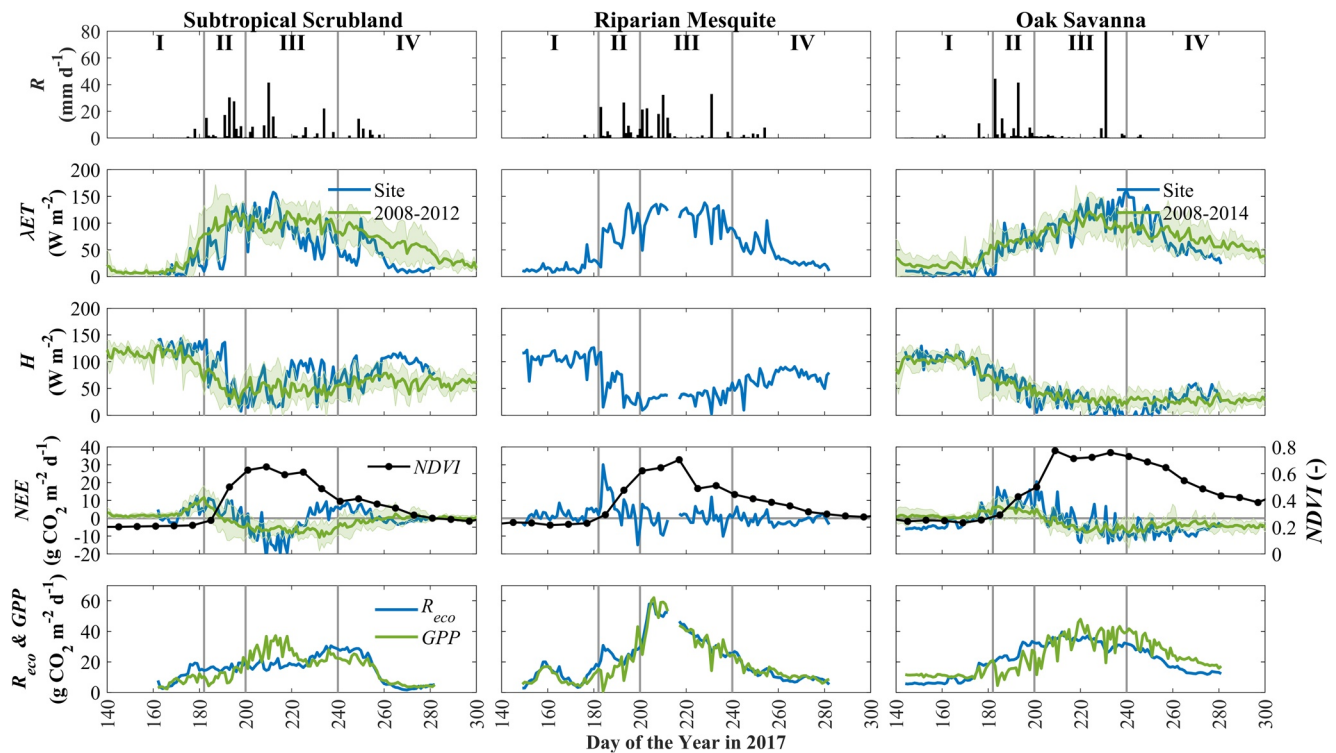
Figure 7. Daily variations of rainfall (R), sensible heat flux (H), latent heat flux (λET), net ecosystem exchange (NEE), ecosystem respiration (R_{eco}), gross primary productivity (GPP), and normalized difference vegetation index (NDVI) at the three study sites and during the NAM stages of: (I) pre-monsoon, (II) early monsoon, (III) late monsoon, and (IV) post-monsoon. Solid lines are values obtained during 2017 (labeled "Site") and solid lines with envelopes are daily averages of previous years with ±1 temporal standard deviation (at SS and OS only).

near surface soil and microclimatic conditions (Verduzco et al., 2018), and a near neutral carbon budget (similar R_{eco} and GPP) for this season. Access to groundwater at the riparian site does not appear sufficient to convert the riparian mesquite into a net carbon sink despite the high ET, as R_{eco} was greater than GPP, consistent with values reported in other riparian mesquites (Scott et al., 2014; Yepez et al., 2007). This is linked to the intensive phenological traits of the riparian mesquite trees. The oak savanna site with access to groundwater and extensive greening is influenced to a lower extent by seasonal rainfall variability and is capable of supporting GPP at higher rates than R_{eco}, in particular for the late-monsoon stage, when it has a supplementary water source. Variations in microclimatic conditions had a small effect on NEE across the gradient, despite influencing GPP and R_{eco}, except at the riparian site where high T_{air}, VPD, and supplemental water co-occur.

4.2. Water Efficiency and Groundwater Contributions

For the conditions of the field campaign, access to groundwater appears to be the more important landscape control on evapotranspiration, though soil and microclimatic conditions modulate the seasonal carbon budget when plants can access deeper subsurface water. For ecosystems dependent on recent rainfall, such as subtropical scrublands, a significant water limitation is present after the end of the NAM, leading to a higher water use efficiency, in particular for the late and post-monsoon stages. A threshold in access to groundwater appears to be required for there to be a transition from intensive to extensive water use strategies. For instance, the riparian site exhibits the phenological traits of intensive water users, but has a much lower water use efficiency due to groundwater access, suggesting that the landscape location did not cross the threshold of available subsurface water. As a result, we infer that a more stable groundwater source is present in the fractured rock of the mountain block such that OS is the only site with plausibly reliable groundwater (e.g., Paco et al., 2009; Rodríguez-Robles et al., 2017), as compared to the lower elevation allu-

Table 5
Direct and Indirect Effects of Soil and Meteorological Variables on ET, NEE, R_{eco}, and GPP From the PA Standardized Path Coefficient (β) for Stages II, III, and IV

	T_{air}			s			VPD
	Direct	Total	Correlation	Direct	Total	Correlation	Direct
SS							
NEE	0.106	0.200	-	−0.066	−0.156	-	0.187
ET	0.272*	0.099	-	0.761*	0.927	-	−0.346*
R_{eco}	0.643*	0.282	-	0.074	0.421	-	−0.723*
GPP	0.483*	0.098	-	0.115	0.485	-	−0.770*
T_{air}	-	-	-	-	-	0.428*	-
s	-	-	0.428*	-	-	-	-
VPD	0.500	-	-	−0.480*	-	-	-
RM							
NEE	0.084	0.303	-	0.574*	0.265	-	0.509*
ET	0.307*	0.124	-	0.627*	0.886	-	−0.426*
R_{eco}	0.171*	0.140	-	0.838*	0.882	-	−0.073
GPP	0.142[X]	0.021	-	0.582*	0.753	-	−0.282[+]
T_{air}	-	-	-	-	-	−0.330*	-
s	-	-	−0.330*	-	-	-	-
VPD	0.430*	-	-	−0.608*	-	-	-
OS							
NEE	0.032	0.067	-	0.473*	0.500	-	0.064
ET	0.394*	−0.016	-	0.171[X]	−0.145	-	−0.745*
R_{eco}	0.448*	0.021	-	0.430*	0.101	-	−0.776*
GPP	0.403*	−0.039	-	0.025	−0.315	-	−0.803*
T_{air}	-	-	-	-	-	−0.480*	-
s	-	-	−0.480*	-	-	-	-
VPD	0.550*	-	-	0.424	-	-	-

Note. Correlation between soil and meteorological variables also tested. * indicates a statistical significance at $p < 0.01$, + at $p < 0.05$, and X at $p < 0.1$.
GPP, gross primary productivity; NEE, net ecosystem exchange; OS, oak savanna; RM, riparian mesquite; SS, subtropical scrubland.

vial aquifers (RM) which are sporadically recharged by ephemeral flooding (e.g., Goodrich et al., 2004; Wilson and Guan, 2004). The riparian mesquite site seems to have intermediate access to groundwater near the ephemeral channel likely after sequences of late monsoon (stage III) storms that could induce streamflow, in contrast to Scott et al. (2014) who found more permanent access near a perennial river.

4.3. Hydrologic Dynamics and Their Link to Carbon Fluxes

Groundwater dependence at riparian and mountain sites link their ecosystem processes to hydrologic dynamics including water table fluctuations, lateral subsurface transport, and episodic recharge (e.g., Eamus et al., 2015; Laio et al., 2009; Martinet et al., 2009). Additional measurements at these sites, including streamflow measurements, sampling of subsurface water levels through piezometers, and water sampling for isotopic analysis, are needed to confirm the hydrologic dynamics identified in this study. At sites with potential groundwater access, evapotranspiration can extend beyond the end of the rainy season, but seasonal carbon budgets depend on the soil and microclimate conditions as well as the plant phenological

Table 6
Seasonal EI, ET_{gw}, and Values of IWUE for Stages II, III, and IV in the Three Ecosystems

	SS	RM	OS
EI (−)			
ET/R	0.83	1.05	1.16
ET/R_c	0.79	1.00	1.11
ET_f/R	0.89	1.23	1.58
ET_f/R_c	0.84	1.17	1.50
ET_{gw} (mm)			
ET_{gw} = ET - R - $Z_r\Delta S$	−47.25	17.81	41.75
ET_{gw} = ET - R_c - $Z_r\Delta S$	−61.05	4.77	28.86
ET_{gw} = ET_f - R - $Z_r\Delta S$	−31.31	64.37	148.42
ET_{gw} = ET_f - R_c - $Z_r\Delta S$	−45.11	51.32	135.53
ET_{gw} = ET - R - $2Z_r\Delta S$	−47.05	23.09	41.24
ET_{gw} = ET_f - R_c - $2Z_r\Delta S$	−44.91	56.61	135.03
IWUE (g CO_2 hPa mm^{-1})			
II	85.06	98.95	97.34
III	120.62	105.18	86.49
IV	247.24	165.47	170.51

EI and ETgw include uncertainty estimates using R_c and ET_f. IWUE, Inherent Water Use Efficiency.

OS, oak savanna; RM, riparian mesquite; SS, subtropical scrubland.

traits. In contrast, subtropical scrublands exhibit evapotranspiration primarily during the rainfall period and showed a nearly neutral seasonal carbon budget for the sampled period. Prior efforts to quantify differences between intensive and extensive water use strategies in the NAM region relied only upon evapotranspiration measurements or remotely-sensed vegetation indices since phenological traits such as the timing of leaf senescence are linked to water use (e.g., Forzieri et al., 2011; Méndez-Barroso et al., 2014). As shown here, the seasonal carbon fluxes provide an important differentiation among sites, in particular that microclimatic conditions and plant water use strategies modulate carbon exchange patterns at sites with access to groundwater. While vegetation indices can be used to distinguish between intensive and extensive greening and provide a long-term context, these observations have limitations in identifying the net seasonal carbon budget across different sites. Additional sampling periods would be needed to identify the inter-annual variability of the carbon budget which has been shown to fluctuate from a net carbon source to a net carbon sink in arid and semiarid ecosystems (e.g., Biederman et al., 2017).

5. Conclusions

In this study, we analyzed the water-energy-carbon fluxes during the North American monsoon of 2017 in three ecosystems of northwestern México. The analysis consisted of an assessment of the field campaign conditions with respect to rainfall data, remotely-sensed vegetation, and flux measurements in the MexFlux database from previous years, which allow inferences to be made across a larger region and across other time periods. We conducted daily analyses during various NAM stages and used a set of indices to determine relations between water and carbon fluxes. We summarize the study conclusions as follows:

1. Rainfall and its subsequent vegetation response during the 2017 NAM season had a similar onset to long-term datasets, but exhibited more (less) pronounced activity in July (August and September), leading to a shorter duration of the NAM. As a consequence, the water-energy-carbon fluxes showed more significant exchanges in the early part of the NAM season and lower activity in the later part, which primarily impacted the lower elevation ecosystem (SS) that depended solely on shallow soil water. Nevertheless, even the high elevation ecosystem with access to groundwater (OS) was influenced to a minor extent by the seasonal rainfall variability.
2. During the field campaign, the ecosystems had a similar rainfall amounts, but differences in access to subsurface water appear to have led to divergent patterns of water and carbon fluxes. Over the study period, low elevation ecosystems with intensive phenological traits were net sources of CO_2 (9.56 and 151.66 g CO_2 m^{-2} at SS and RM), while the high elevation ecosystem (OS) with an extensive plant strategy acted as a net carbon sink of −299.25 g CO_2 m^{-2}. This suggest that soil (*s*) and microclimatic (T_{air}, VPD) conditions modulated the seasonal carbon budget through differential effects on ecosystem respiration and gross primary productivity. In addition, extended leaf phenology at OS allowed for continued productivity during the post-monsoon stage when ecosystem respiration became more subdued with decreases in *s* and T_{air}.
3. Elevation-induced soil and microclimate conditions varied in their influence on water-energy-carbon fluxes at the sites, as revealed by the path analysis. As air temperature increased at all sites, we noted a statistically significant increase in evapotranspiration and carbon flux components, but a weak influence on net ecosystem exchange. The effect of VPD on NEE was only statistically significant at the riparian mesquite site, where there was co-occurrence of high air temperature, atmospheric demand, and supplemental water sources. Higher soil water content was positively correlated to evapotranspiration at all
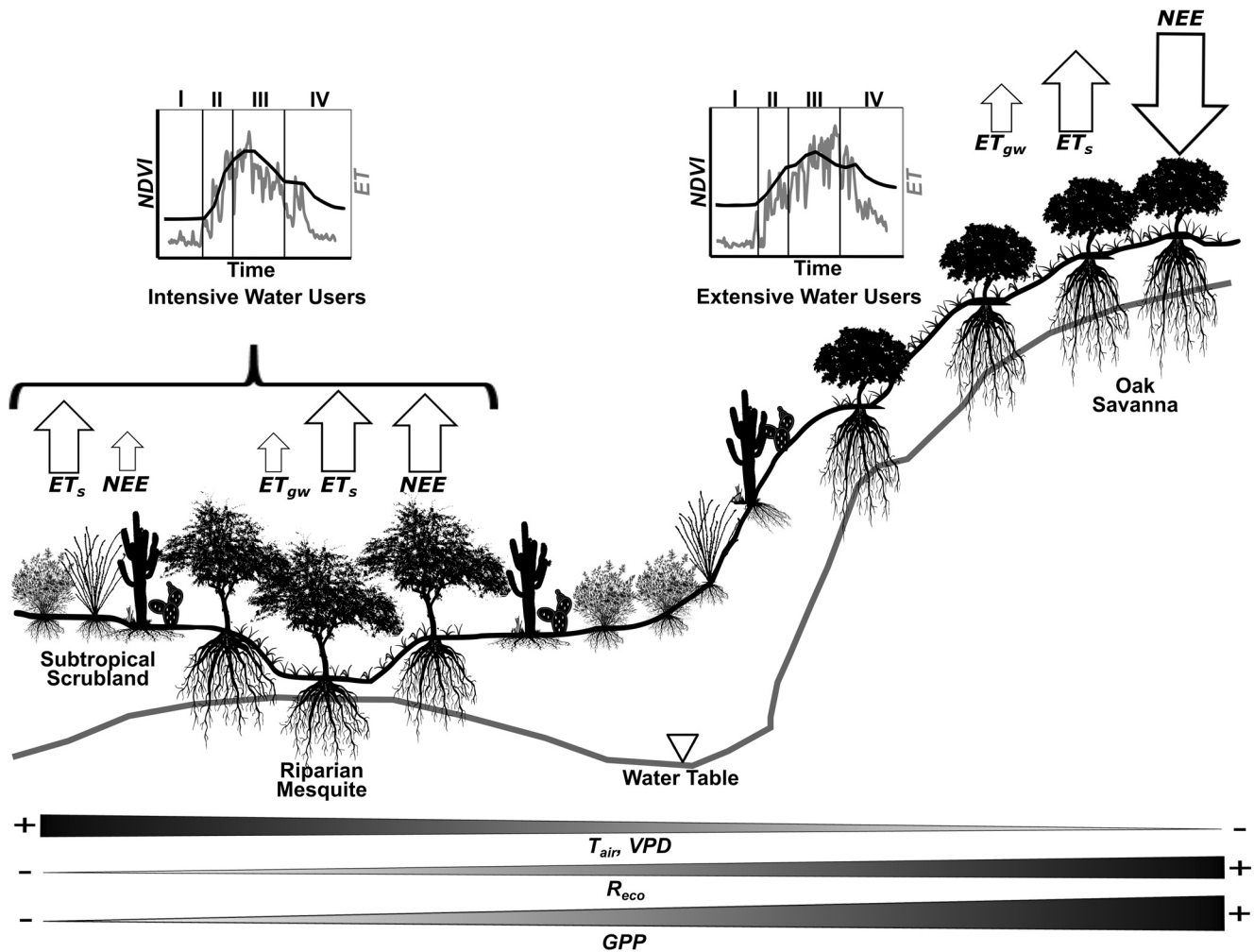
Figure 8. Schematic of the effect of landscape controls, including microclimatic conditions and access to groundwater, on water-energy-carbon fluxes during the North American monsoon for intensive and extensive water use strategies. Schematic is not to scale.

sites, while CO_2 release (higher R_{eco} and NEE) was promoted with higher s only for sites with access to groundwater where vegetation and microbial activity was likely to be promoted.

4. Estimates of groundwater used for evapotranspiration varied significantly among the ecosystems such that deeper sources were likely consumed at the riparian and mountain settings. This was accompanied by differences in water use efficiency, with subtropical scrublands having higher efficiency under water stressed conditions. In contrast, groundwater access allows riparian mesquites and oak savannas to have lower efficiencies at the end of the rainy season. Inferences from the water-energy-carbon fluxes indicate that a more stable groundwater source is likely present at the mountain block site as compared to the site in an alluvial aquifer.

Despite the long-term context provided, the study outcomes remain conditioned on a single NAM season, suggesting that additional field monitoring is warranted across the seasonally dry ecosystem gradient, in particular given the high inter-annual variability of the NAM (e.g., Gutzler, 2004; Forzieri et al., 2011). Verduzco et al. (2015), for instance, identified large inter-annual differences in net seasonal carbon budgets due to variations in NAM rainfall amounts as well as the effects of the preceding winter. As such, we could expect variations in the relative roles of access to groundwater and microclimatic conditions driven by changes in rainfall availability. While previous MexFlux datasets are helpful as shown here, these do not contain the riparian mesquite woodland that serves as an important intermediate site, with both access to groundwater and the soil and microclimatic conditions of low elevation areas.

Future work should consider the permanent installation of water-energy-carbon flux sites across an ecosystem gradient that exposes differences in landscape controls in a structured manner, including a mountain site without access to groundwater to serve as an additional comparative location. Finding sites that isolate a particular landscape control, for instance an elevation effect, without the concomitant presence of another control, for instance access to groundwater, is difficult. However, such EC sites would potentially reveal if groundwater access provides a stabilizing role to the seasonal and annual water and carbon budgets in the midst of the high inter-annual rainfall variability as well as the legacy effects previously noted between winter and summer seasons (e.g., Delgado-Balbuena, Yepez, et al., 2019; Verduzco et al., 2015). This is particularly relevant given anticipated changes in seasonal rainfall due to climate change in the NAM region (e.g.,Cook & Seager, 2013; Pascale et al., 2019; Seager et al., 2007). Under scenarios of lower rainfall amounts delivered as more extreme events, we anticipate that ecosystems with access to groundwater will rely more heavily on this source to sustain evapotranspiration and carbon uptake during the NAM. In contrast, ecosystems with intensive water use strategies will require adjustments via higher water use efficiency to avoid a reorganization of plant assemblages.

Data Availability Statement

Datasets on precipitation, meteorological conditions and water-energy-carbon fluxes are available through Zenodo (Pérez-Ruiz & Vivoni, 2019), available at: http://doi.org/10.5281/zenodo.3522331.

References

Adams, D. K., & Comrie, A. C. (1997). The north American monsoon. *Bulletin of the American Meteorological Society*, *78*, 2197–2213. https://doi.org/10.1175/1520-0477(1997)078<2197:tnam>2.0.co;2

Ahlström, A., Raupach, M. R., Schurgers, G., Smith, B., Arneth, A., Jung, M., et al. (2015). The dominant role of semi-arid ecosystems in the trend and variability of the land CO_2 sink. *Science*, *348*, 895–899. https://doi.org/10.1126/science.aaa1668

Baldocchi, D., Falge, E., Gu, L., Olson, R., Hollinger, D., Running, S., et al. (2001). FLUXNET: A new tool to study the temporal and spatial variability of ecosystem-scale carbon dioxide, water vapor, and energy flux densities. *Bulletin of the American Meteorological Society*, *82*(11), 2415–2434. https://doi.org/10.1175/1520-0477(2001)082<2415:fantts>2.3.co;2

Baldocchi, D. D. (2003). Assessing the eddy covariance technique for evaluating carbon dioxide exchange rates of ecosystems: Past, present and future. *Global Change Biology*, *9*(4), 479–492. https://doi.org/10.1046/j.1365-2486.2003.00629.x

Baldocchi, D. D., Xu, L., & Kiang, N. (2004). How plant functional-type, weather, seasonal drought, and soil physical properties alter water and energy fluxes of an oak-grass Savanna and an annual grassland. *Agricultural and Forest Meteorology*, *123*, 13–39. https://doi.org/10.1016/j.agrformet.2003.11.006

Barron-Gafford, G. A., Scott, R. L., Jenerette, G. D., Hamerlynck, E. P., & Huxman, T. E. (2013). Landscape and environmental controls over leaf and ecosystem carbon dioxide fluxes under woody plant expansion. *Journal of Ecology*, *101*(6), 1471–1483.

Beer, C., Ciais, P., Reichstein, M., Baldocchi, D., Law, B. E., Papale, D., et al. (2009). Temporal and among-site variability of inherent water use efficiency at the ecosystem level. *Global Biogeochemical Cycles*, *23*(2), GB2018. https://doi.org/10.1029/2008GB003233

Biederman, J. A., Scott, R. L., Arnone, III, J. A., III, Jasoni, R. L., Litvak, M. E., Moreo, M. T., et al. (2018). Shrubland carbon sink depends upon winter water availability in the warm deserts of North America. *Agricultural and Forest Meteorology*, *249*, 407–419. https://doi.org/10.1016/j.agrformet.2017.11.005

Biederman, J. A., Scott, R. L., Bell, T. W., Bowling, D. R., Dore, S., Garatuza-Payan, J., et al. (2017). CO_2 exchange and evapotranspiration across dryland ecosystems of southwestern North America. *Global Change Biology*, *23*(10), 4204–4221. https://doi.org/10.1111/gcb.13686

Bowling, D. R., Bethers-Marchetti, S., Lunch, C. K., Grote, E. E., & Belnap, J. (2010). Carbon, water, and energy fluxes in a semiarid cold desert grassland during and following multiyear drought. *Journal of Geophysical Research*, *115*(G4), G04026. https://doi.org/10.1029/2010JG001322

Brunel, J.-P. (2009). Sources of water used by natural mesquite vegetation in a semi-arid region of northern Mexico. *Hydrological Sciences Journal*, *54*(2), 375–381. https://doi.org/10.1623/hysj.54.2.375

Budyko, M. I. (1974). *Climate and life* (p. 508). New York, NY: Academic Press.

Cable, D. R. (1977). Seasonal use of soil water by mature velvet mesquite. *Journal of Range Management*, *30*, 4–11. https://doi.org/10.2307/3897324

Cavazos, T., Comrie, A. C., & Liverman, D. M. (2002). Intraseasonal variability associated with wet monsoons in southeast Arizona. *Journal of Climate*, *15*(17), 2477–2490. https://doi.org/10.1175/1520-0442(2002)015<2477:ivawwm>2.0.co;2

Cook, B. I., & Seager, R. (2013). The response of the north American monsoon to increased greenhouse gas forcing. *Journal of Geophysical Research: Atmospheres*, *118*(4), 1690–1699. https://doi.org/10.1002/jgrd.50111

Delgado-Balbuena, J., Arredondo, J. T., Loescher, H. W., Pineda-Martinez, L. F., Carbajal, J. N., & Vargas, R. (2019). Seasonal precipitation legacy effects determine the carbon balance of a semiarid grassland. *Journal of Geophysical Research: Biogeosciences*, *124*(4), 987–1000.

Delgado-Balbuena, J., Yépez, E. A., Paz-Pellat, F., Ángeles-Pérez, G., Aguirre-Gutiérrez, C., Alvarado-Barrientos, M. S., et al. (2019). Base de datos de flujos verticales de dioxido de carbono en ecosistemas terrestres y costeros en México. *Elementos para Políticas Públicas.*, *2*(2), 93–108.

Douglas, M. W., Maddox, R. A., Howard, K., & Reyes, S. (1993). The Mexican monsoon. *Journal of Climate*, *6*(8), 1665–1677. https://doi.org/10.1175/1520-0442(1993)006<1665:tmm>2.0.co;2

Eamus, D., Zolfaghar, S., Villalobos-Vega, R., Cleverly, J., & Huete, A. (2015). Groundwater-dependent ecosystems: Recent insights from satellite and field-based studies. *Hydrology and Earth System Sciences*, *19*, 4229–4256. https://doi.org/10.5194/hess-19-4229-2015

Foken, T. (2006). 50 Years of the Monin-Obukhov similarity theory. *Boundary-Layer Meteorology*, *119*, 431–447. https://doi.org/10.1007/s10546-006-9048-6

Forzieri, G., Castelli, F., & Vivoni, E. R. (2011). Vegetation dynamics within the north American monsoon region. *Journal of Climate*, *24*(6), 1763–1783. https://doi.org/10.1175/2010jcli3847.1

Forzieri, G., Feyen, L., Cescatti, A., & Vivoni, E. R. (2014). Spatial and temporal variations in ecosystem response to monsoon precipitation variability in southwestern North America. *Journal of Geophysical Research: Biogeoscience*, *119*(10), 1999–2017. https://doi.org/10.1002/2014jg002710

Goodrich, D. C., Williams, D. G., Unkrich, C. L., Hogan, J. F., Scott, R. L., Hultine, K. R., et al. (2004). Comparison of methods to estimate ephemeral channel recharge, Walnut Gulch, San Pedro River Basin, Arizona. In F. Phillips, J. Hogan, & B. Scanlon (Eds.), *Groundwater recharge in a desert environment, the southwestern United States*. Washington, WA: American Geophysical Union. https://doi.org/10.1029/009WSA08

Gutzler, D. S. (2004). An index of interannual precipitation variability in the core of the North American monsoon region. *Journal of Climate*, *17*, 4473–4480. https://doi.org/10.1175/3226.1

Higgins, R. W., Chen, Y., & Douglas, A. V. (1999). Interannual variability of the North American warm season precipitation regime. *Journal of Climate*, *12*(3), 653–680. https://doi.org/10.1175/1520-0442(1999)012<0653:ivotna>2.0.co;2

Hinojo-Hinojo, C., Castellanos, A. E., Huxman, T., Rodriguez, J. C., Vargas, R., Romo-León, J. R., & Biederman, J. A. (2019). Native shrubland and managed buffelgrass savanna in drylands: Implications for ecosystem carbon and water fluxes. *Agricultural and Forest Meteorology*, *268*, 269–278. https://doi.org/10.1016/j.agrformet.2019.01.030

Hinojo-Hinojo, C., Castellanos, A. E., Rodríguez, J. C., Delgado-Balbuena, J., Romo-León, J. R., Celaya-Michel, H., & Huxman, T. E. (2016). Carbon and water fluxes in an exotic buffelgrass savanna. *Rangeland Ecology & Management*, *69*(5), 334–341. https://doi.org/10.1016/j.rama.2016.04.002

Hui, D., Luo, Y., & Katul, G. (2003). Partitioning interannual variability in net ecosystem exchange between climatic variability and functional change. *Tree Physiology*, *23*(7), 433–442. https://doi.org/10.1093/treephys/23.7.433

Huxman, T. E., Turnipseed, A. A., Sparks, J. P., Harley, P. C., & Monson, R. K. (2003). Temperature as a control over ecosystem CO_2 fluxes in a high-elevation, subalpine forest. *Oecologia*, *134*(4), 537–546. https://doi.org/10.1007/s00442-002-1131-1

INEGI (2016). Conjunto de Datos Vectoriales de Uso de Suelo y Vegetación. Escala 1:250 000. Serie VI. Edición: 1. Clave H1208. Aguascalientes: Instituto Nacional de Estadística y Geografía.

Jia, X., Zha, T. S., Wu, B., Zhang, Y. Q., Gong, J. N., Qin, S. G., et al. (2014). Biophysical controls on net ecosystem CO_2 exchange over a semiarid Shrubland in northwest China. *Biogeosciences*, *4679*.

Kljun, N., Calanca, P., Rotach, M. W., & Schmid, H. P. (2015). A simple two-dimensional parameterisation for flux footprint prediction (FFP). *Geoscientific Model Development*, *8*(11), 3695–3713. https://doi.org/10.5194/gmd-8-3695-2015

Knowles, J. F., Scott, R. L., Minor, R. L., & Barron-Gafford, G. A. (2020). Ecosystem carbon and water cycling from a sky island montane forest. *Agricultural and Forest Meteorology*, *281*, 107835. https://doi.org/10.1016/j.agrformet.2019.107835

Ko, A., Mascaro, G., & Vivoni, E. R. (2019). Strategies to improve and evaluate physics-based hyperresolution hydrologic simulations at regional basin scales. *Water Resources Research*, *55*(2), 1129–1152. https://doi.org/10.1029/2018wr023521

Kurc, S. A., & Small, E. E. (2007). Soil moisture variations and ecosystem-scale fluxes of water and carbon in semiarid grassland and shrubland. *Water Resources Research*, *43*(6), W06416. https://doi.org/10.1029/2006WR005011

Lagergren, F., Lindroth, A., Dellwik, E., Ibrom, A., Lankreijer, H., Launiainen, S., et al. (2008). Biophysical controls on CO_2 fluxes of three northern forests based on long-term eddy covariance data. *Tellus B: Chemical and Physical Meteorology*, *60*(2), 143–152. https://doi.org/10.1111/j.1600-0889.2006.00324.x

Laio, F., Tamea, S., Ridolfi, L., D'Odorico, P., & Rodriguez-Iturbe, I. (2009). Ecohydrology of groundwater-dependent ecosystems: 1. Stochastic water table dynamics. *Water Resources Research*, *45*, W05419. https://doi.org/10.1029/2008WR007292

Li, G., Han, H., Du, Y., Hui, D., Xia, J., Niu, S., et al. (2017). Effects of warming and increased precipitation on net ecosystem productivity: A long-term manipulative experiment in a semiarid grassland. *Agricultural and Forest Meteorology*, *232*, 359–366. https://doi.org/10.1016/j.agrformet.2016.09.004

Lizárraga-Celaya, C., Watts, C. J., Rodríguez, J. C., Garatuza-Payán, J., Scott, R. L., & Sáiz-Hernández, J. (2010). Spatio-temporal variations in surface characteristics over the North American monsoon region. *Journal of Arid Environments*, *74*(5), 540–548. https://doi.org/10.1016/j.jaridenv.2009.09.027

Lloyd, J., & Taylor, J. A. (1994). On the temperature dependence of soil respiration. *Functional Ecology*, *8*(3), 315–323. https://doi.org/10.2307/2389824

Martinet, M. C., Vivoni, E. R., Cleverly, J. R., Thibault, J. R., Schuetz, J. F., & Dahm, C. N. (2009). On groundwater fluctuations, evapotranspiration, and understory removal in riparian corridors. *Water Resources Research*, *45*, W05425. https://doi.org/10.1029/2008WR007152

Mascaro, G., Vivoni, E. R., Gochis, D. J., Watts, C. J., & Rodríguez, J. C. (2014). Temporal downscaling and statistical analysis of rainfall across a topographic transect in northwest Mexico. *Journal of Applied Meteorology and Climatology*, *53*(4), 910–927. https://doi.org/10.1175/jamc-d-13-0330.1

Massman, W. J. (2001). Reply to comment by Rannik on "A simple method for estimating frequency response corrections for eddy covariance systems". *Agricultural and Forest Meteorology*, *107*, 247–251. https://doi.org/10.1016/s0168-1923(00)00237-9

Méndez-Barroso, L. A., & Vivoni, E. R. (2010). Observed shifts in land surface conditions during the North American monsoon: Implications for a vegetation-rainfall feedback mechanism. *Journal of Arid Environments*, *74*(5), 549–555. https://doi.org/10.1016/j.jaridenv.2009.09.026

Méndez-Barroso, L. A., Vivoni, E. R., Robles-Morua, A., Mascaro, G., Yépez, E. A., Rodríguez, J. C., et al. (2014). A modeling approach reveals differences in evapotranspiration and its partitioning in two semiarid ecosystems in northwest Mexico. *Water Resources Research*, *50*(4), 3229–3252. https://doi.org/10.1002/2013wr014838

Méndez-Barroso, L. A., Vivoni, E. R., Watts, C. J., & Rodríguez, J. C. (2009). Seasonal and interannual relations between precipitation, surface soil moisture and vegetation dynamics in the North American monsoon region. *Journal of Hydrology*, *377*, 59–70. https://doi.org/10.1016/j.jhydrol.2009.08.009

Moncrieff, J. B., Massheder, J. M., De Bruin, H., Elbers, J., Friborg, T., Heusinkveld, B., et al. (1997). A system to measure surface fluxes of momentum, sensible heat, water vapour and carbon dioxide. *Journal of Hydrology*, *188–189*, 589–611. https://doi.org/10.1016/s0022-1694(96)03194-0

Moncrieff, J., Clement, R., Finnigan, J., & Meyers, T. (2004). Averaging, detrending, and filtering of eddy covariance time series. In Law, B. E., Lee, X., Massman, W. J. (Eds.), *Handbook of micrometeorology* (pp. 7–31). Dordrecht: Springer.

Monson, R. K., Sparks, J. P., Rosenstiel, T. N., Scott-Denton, L. E., Huxman, T. E., Harley, P. C., et al. (2005). Climatic influences on net ecosystem CO_2 exchange during the transition from wintertime carbon source to springtime carbon sink in a high-elevation, subalpine forest. *Oecologia*, *146*(1), 130–147. https://doi.org/10.1007/s00442-005-0169-2

Nakai, T., & Shimoyama, K. (2012). Ultrasonic anemometer angle of attack errors under turbulent conditions. *Agricultural and Forest Meteorology*, *162–163*, 14–26. https://doi.org/10.1016/j.agrformet.2012.04.004

ORNL DAAC. (2018). MODIS and VIIRS Land Products Global Subsetting and Visualization Tool. ORNL DAAC, Oak Ridge, Tennessee, USA. Accessed April 04, 2019. Subset obtained for MOD13Q1 product at 29.8297N,110.5032W, time period: 2000-02-18 to 2019-03-06, and subset size: 100.25 x 100.25 km. Retrieved from https://doi.org/10.3334/ORNLDAAC/1379

Paço, T. A., David, T. S., Henriques, M. O., Pereira, J. S., Valente, F., Banza, J., et al. (2009). Evapotranspiration from a Mediterranean evergreen oak savannah: The role of trees and pasture. *Journal of Hydrology*, *369*, 98–106. https://doi.org/10.1016/j.jhydrol.2009.02.011

Papale, D., Reichstein, M., Aubinet, M., Canfora, E., Bernhofer, C., Kutsch, W., et al. (2006). Towards a standardized processing of net ecosystem exchange measured with eddy covariance technique: Algorithms and uncertainty estimation. *Biogeosciences*, *3*(4), 571–583. https://doi.org/10.5194/bg-3-571-2006

Pascale, S., Carvalho, L. M. V., Adams, D. K., Castro, C. L., & Cavalcanti, I. F. A. (2019). Current and future variations of the monsoons of the Americas in a warming climate. *Current Climate Change Reports*, *5*(3), 125–144. https://doi.org/10.1007/s40641-019-00135-w

Paw U, K. T., Baldocchi, D. D., Meyers, T. P., & Wilson, K. B. (2000). Correction of eddy-covariance measurements incorporating both advective effects and density fluxes. *Boundary-Layer Meteorology*, *97*, 487–511. https://doi.org/10.1023/a:1002786702909

Peel, M. C., Finlayson, B. L., & McMahon, T. A. (2007). Updated world map of the Köppen-Geiger climate classification. *Hydrology and Earth System Sciences*, *11*, 1633–1644. https://doi.org/10.5194/hess-11-1633-2007

Pérez-Ruiz, E. R., Garatuza-Payan, J., Watts, C. J., Rodriguez, J. C., Yépez, E. A., & Scott, R. L. (2010). Carbon dioxide and water vapour exchange in a tropical dry forest as influenced by the North American Monsoon System (NAMS). *Journal of Arid Environments*, *74*(5), 556–563. https://doi.org/10.1016/j.jaridenv.2009.09.029

Pérez-Ruiz, E. R., & Vivoni, E. R. (2019). *The North American monsoon GPS hydrometeorological network 2017: Flux and precipitation data [Data set]*. Zenodo. https://doi.org/10.5281/zenodo.3522331

Potts, A., Scott, R. L., Bayram, S., & Carbonara, J. (2010). Woody plants modulate the temporal dynamics of soil moisture in a semi-arid mesquite savanna. *Ecohydrology*, *3*(1), 20–34. https://doi.org/10.2307/book5.7

Potts, D. L., Scott, R. L., Cable, J. M., Huxman, T. E., & Williams, D. G. (2008). Sensitivity of mesquite shrubland CO_2 exchange to precipitation in contrasting landscape settings. *Ecology*, *89*(10), 2900–2910. https://doi.org/10.1890/07-1177.1

Poulter, B., Frank, D., Ciais, P., Myneni, R. B., Andela, N., Bi, J., et al. (2014). Contribution of semi-arid ecosystems to interannual variability of the global carbon cycle. *Nature*, *509*(7502), 600–603. https://doi.org/10.1038/nature13376

Reichstein, M., Falge, E., Baldocchi, D., Papale, D., Aubinet, M., Berbigier, P., et al. (2005). On the separation of net ecosystem exchange into assimilation and ecosystem respiration: Review and improved algorithm. *Global Change Biology*, *11*(9), 1424–1439. https://doi.org/10.1111/j.1365-2486.2005.001002.x

Rodriguez-Iturbe, I., Porporato, A., Laio, F., & Ridolfi, L. (2001). Intensive or extensive use of soil moisture: Plant strategies to cope with stochastic water availability. *Geophysical Research Letters*, *28*(23), 4495–4497.

Rodríguez-Robles, U., Arredondo, T., Huber-Sannwald, E., Ramos-Leal, J. A., & Yépez, E. A. (2017). Technical note: Application of geophysical tools for tree root studies in forest ecosystems in complex soils. *Biogeosciences*, *14*, 5343–5357. https://doi.org/10.5194/bg-14-5343-2017

Rojas-Robles, N. E., Garatuza-Payán, J., Álvarez-Yépiz, J. C., Sánchez-Mejía, Z. M., Vargas, R., & Yépez, E. A. (2020). Environmental controls on carbon and water fluxes in an old-growth tropical dry forest. *Journal of Geophysical Research: Biogeosciences*, *125*(8), e2020JG005666.

Saito, M., Kato, T., & Tang, Y. (2009). Temperature controls ecosystem CO_2 exchange of an alpine meadow on the northeastern Tibetan Plateau. *Global Change Biology*, *15*(1), 221–228. https://doi.org/10.1111/j.1365-2486.2008.01713.x

Schenk, H. J., & Jackson, R. B. (2002). The global biogeography of roots. *Ecological Monographs*, *72*(3), 311–328. https://doi.org/10.1890/0012-9615(2002)072[0311:tgbor]2.0.co;2

Schmid, H., Grimmond, C. S. B., Cropley, F., Offerle, B., & Su, H. B. (2000). Measurements of CO_2 and energy fluxes over a mixed hardwood forest in the mid-western United States. *Agricultural and Forest Meteorology*, *103*(4), 357–374. https://doi.org/10.1016/s0168-1923(00)00140-4

Schreiner-McGraw, A. P., & Vivoni, E. R. (2018). On the sensitivity of hillslope runoff and channel transmission losses in arid piedmont slopes. *Water Resources Research*, *54*(7), 4498–4518.

Scott, R. L. (2010). Using watershed water balance to evaluate the accuracy of eddy covariance evaporation measurements for three semi-arid ecosystems. *Agricultural and Forest Meteorology*, *150*(2), 219–225. https://doi.org/10.1016/j.agrformet.2009.11.002

Scott, R. L., Cable, W. L., Huxman, T. E., Nagler, P. L., Hernandez, M., & Goodrich, D. C. (2008). Multiyear riparian evapotranspiration and groundwater use for a semiarid watershed. *Journal of Arid Environments*, *72*(7), 1232–1246. https://doi.org/10.1016/j.jaridenv.2008.01.001

Scott, R. L., Edwards, E. A., Shuttleworth, W. J., Huxman, T. E., Watts, C. J., & Goodrich, D. C. (2004). Interannual and seasonal variation in fluxes of water and carbon dioxide from a riparian woodland ecosystem. *Agricultural and Forest Meteorology*, *122*(1–2), 65–84. https://doi.org/10.1016/j.agrformet.2003.09.001

Scott, R. L., Hamerlynck, E. P., Jenerette, G. D., Moran, M. S., & Barron-Gafford, G. A. (2010). Carbon dioxide exchange in a semidesert grassland through drought-induced vegetation change. *Journal of Geophysical Research*, *115*, G03026. https://doi.org/10.1029/2010JG001348

Scott, R. L., Huxman, T. E., Barron-Gafford, G. A., Darrel Jenerette, G., Young, J. M., & Hamerlynck, E. P. (2014). When vegetation change alters ecosystem water availability. *Global Change Biology*, *20*(7), 2198–2210. https://doi.org/10.1111/gcb.12511

Scott, R. L., Jenerette, G. D., Potts, D. L., & Huxman, T. E. (2009). Effects of seasonal drought on net carbon dioxide exchange from a woody-plant-encroached semiarid grassland. *Journal of Geophysical Research*, *114*, G04004. https://doi.org/10.1029/2008JG000900

Seager, R., Ting, M., Held, I., Kushnir, Y., Lu, J., Vecchi, G., et al. (2007). Model projections of an imminent transition to a more arid climate in southwestern North America. *Science*, *316*(5828), 1181–1184. https://doi.org/10.1126/science.1139601

Shao, J., Zhou, X., Luo, Y., Li, B., Aurela, M., Billesbach, D., et al. (2016). Direct and indirect effects of climatic variations on the interannual variability in net ecosystem exchange across terrestrial ecosystems. *Tellus B: Chemical and Physical Meteorology*, *68*(1), 30575. https://doi.org/10.3402/tellusb.v68.30575

Tarín, T., Yépez, E. A., Garatuza-Payán, J., Rodríguez, J. C., Méndez-Barroso, L. A., Watts, C. J., & Vivoni, E. R. (2020). Evapotranspiration flux partitioning at multi-species shrubland with stable isotopes of soil, plant, and atmospheric water pools. *Atmósfera*, *33*(4), 319–335.

Twine, T. E., Kustas, W. P., Norman, J. M., Cook, D. R., Houser, P. R., Meyers, T. P., et al. (2000). Correcting eddy-covariance flux underestimates over a grassland. *Agricultural and Forest Meteorology*, *103*(3), 279–300. https://doi.org/10.1016/s0168-1923(00)00123-4

Vargas, R., Yépez, E. A., Andrade, J. L., Ángeles, G., Arredondo, T., Castellanos, A. E., et al. (2013). Progress and opportunities for monitoring greenhouse gases fluxes in Mexican ecosystems: The MexFlux network. *Atmósfera*, *26*(3), 325–336. https://doi.org/10.1016/s0187-6236(13)71079-8

Verduzco, V. S., Garatuza-Payán, J., Yépez, E. A., Watts, C. J., Rodríguez, J. C., Robles-Morua, A., & Vivoni, E. R. (2015). Variations of net ecosystem production due to seasonal precipitation differences in a tropical dry forest of northwest Mexico. *Journal of Geophysical Research: Biogeosciences*, *120*(10), 2081–2094. https://doi.org/10.1002/2015jg003119

Verduzco, V. S., Vivoni, E. R., Yépez, E. A., Rodríguez, J. C., Watts, C. J., Tarín, T., et al. (2018). Climate change impacts on net ecosystem productivity in a subtropical Shrubland of northwestern México. *Journal of Geophysical Research: Biogeosciences.*, *123*(2), 688–711. https://doi.org/10.1002/2017jg004361

Vickers, D., & Mahrt, L. (1997). Quality control and flux sampling problems for tower and aircraft data. *Journal of Atmospheric and Oceanic Technology*, *14*(3), 512–526. https://doi.org/10.1175/1520-0426(1997)014<0512:qcafsp>2.0.co;2

Vivoni, E. R., Gutiérrez-Jurado, H. A., Aragón, C. A., Méndez-Barroso, L. A., Rinehart, A. J., Wyckoff, R. L., et al. (2007). Variation of hydrometeorological conditions along a topographic transect in northwestern Mexico during the north American monsoon. *Journal of Climate*, *20*(9), 1792–1809. https://doi.org/10.1175/jcli4094.1

Vivoni, E. R., Moreno, H. A., Mascaro, G., Rodriguez, J. C., Watts, C. J., Garatuza-Payan, J., & Scott, R. L. (2008). Observed relation between evapotranspiration and soil moisture in the North American monsoon region. *Geophysical Research Letters*, *35*, L22403. https://doi.org/10.1029/2008GL036001

Vivoni, E. R., Pérez-Ruiz, E. R., Keller, Z. T., Escoto, E. A., Templeton, R. C., Templeton, N. P., et al. (2021). Long-term research catchments to investigate shrub encroachment in the Sonoran and Chihuahuan deserts: Santa Rita and Jornada experimental ranges. *Hydrological Processes*, *35*. https://doi.org/10.1002/hyp.14031

Vivoni, E. R., Rodríguez, J. C., & Watts, C. J. (2010). On the spatiotemporal variability of soil moisture and evapotranspiration in a mountainous basin within the North American monsoon region. *Water Resources Research*, *46*, W02509. https://doi.org/10.1029/2009WR008240

Wang, S., Zhang, Y., Lü, S., Su, P., Shang, L., & Li, Z. (2016). Biophysical regulation of carbon fluxes over an alpine meadow ecosystem in the eastern Tibetan Plateau. *International Journal of Biometeorology*, *60*(6), 801–812. https://doi.org/10.1007/s00484-015-1074-y

Wang, Y. F., Cui, X. Y., Hao, Y. B., Mei, X. R., Yu, G. R., Huang, X. Z., et al. (2011). The fluxes of CO_2 from grazed and fenced temperate steppe during two drought years on the Inner Mongolia Plateau, China. *Science of the Total Environment*, *410*, 182–190.

Webb, E. K., Pearman, G. I., & Leuning, R. (1980). Correction of flux measurements for density effects due to heat and water vapour transfer. *Quarterly Journal of the Royal Meteorological Society*, *106*, 85–100. https://doi.org/10.1002/qj.49710644707

Westenburg, C. L., Harper, D. P., & DeMeo, G. A. (2006). *Evapotranspiration by phreatophytes along the lower Colorado River at Havasu national wildlife refuge, Arizona*. US Geological Survey Scientific Investigations Report 2006–5043, (p. 44).

Wilczak, J. M., Oncley, S. P., & Stage, S. A. (2001). Sonic anemometer tilt correction algorithms. *Boundary-Layer Meteorology*, *99*, 127–150. https://doi.org/10.1023/a:1018966204465

Williams, C. A., Reichstein, M., Buchmann, N., Baldocchi, D., Beer, C., Schwalm, C., et al. (2012). Climate and vegetation controls on the surface water balance: Synthesis of evapotranspiration measured across a global network of flux towers. *Water Resources Research*, *48*, W06523. https://doi.org/10.1029/2011WR011586

Williams, D. G., Scott, R. L., Huxman, T. E., Goodrich, D. C., & Lin, G. (2006). Sensitivity of riparian ecosystems in arid and semiarid environments to moisture pulses. *Hydrological Processes*, *20*(15), 3191–3205. https://doi.org/10.1002/hyp.6327

Wilson, J. L., & Guan, H. (2004). Mountain-block hydrology and mountain-front recharge. In F. Phillips, J. Hogan, & B. Scanlon (Eds.), *Groundwater recharge in a desert environment, the southwestern United States* (pp. 113–137). Washington, WA: American Geophysical Union. https://doi.org/10.1029/009WSA08

Wilson, K., Goldstein, A., Falge, E., Aubinet, M., Baldocchi, D., Berbigier, P., et al. (2002). Energy balance closure at FLUXNET sites. *Agricultural and Forest Meteorology*, *113*(1–4), 223–243. https://doi.org/10.1016/s0168-1923(02)00109-0

Wutzler, T., Lucas-Moffat, A., Migliavacca, M., Knauer, J., Sickel, K., Šigut, L., et al. (2018). Basic and extensible post-processing of eddy covariance flux data with REddyProc. *Biogeosciences*, *15*(16), 5015–5030. https://doi.org/10.5194/bg-15-5015-2018

Yépez, E. A., Scott, R. L., Cable, W. L., & Williams, D. G. (2007). Intraseasonal variation in water and carbon dioxide flux components in a semiarid riparian woodland. *Ecosystems*, *10*, 1100–1115. https://doi.org/10.1007/s10021-007-9079-y